博士論文

Structural control of nitride semiconductors and its application to light emitting devices

（窒化物半導体成長における構造制御と発光素子への応用）

孫 政佑

Abstract

Group III nitride semiconductors are promising materials for high efficiency light emitting devices because of their excellent properties. Single crystalline sapphire substrates have been used to fabricate GaN-based devices owing to their high thermal stability and high crystalline quality. On the other hand, the applications of GaN-based devices have been limited by the unavailability of large crystals and the high fabrication cost of sapphire substrates. Therefore, many researchers have worked to develop new substrates, such as amorphous SiO_2, metal foils, and other oxide crystals. Amongst these studies, flat glass is an ideal substrate material for future LEDs because of its scalability and low cost. Despite the advantages of glass, there are two serious problems that have impeded its use as a substrate for GaN films. The first problem is the amorphous nature of glass, where GaN films grown on glass have poor crystalline quality. To overcome this problem, the introduction of crystalline buffer layers is required before the growth of GaN films. Graphene is a suitable material as the buffer layers for the GaN growth, because large-area multi-layer graphene films with highly c-axis oriented structures are available and can be transferred easily to glass substrates. The second problem is the low softening temperature of glass. Glass cannot be used as a substrate for GaN growth because the substrate temperature for GaN growth is normally above 1000°C in conventional metalorganic chemical vapor deposition (MOCVD). Fortunately, recent progress in epitaxial growth techniques based on pulsed sputtering deposition (PSD) has enabled the growth of group III nitrides, even at room temperatures. This successful reduction in growth temperature is attributed to the high kinetic energy and the pulsed supply of group III atoms, which assist the

surface migration of the film precursors on the substrate surfaces. This striking nature of PSD might allow the fabrication of nitride devices even below the softening temperature of flat glass in the future.

Therefore, this study assessed the feasibility of nitride crystal growth on SiO_2 with MLG buffer layers grown by PSD as well as the application of this structure to the fabrication of LEDs. The structural characterization of the GaN films on these substrates showed that the use of a multi layer graphene (MLG) buffer layer imposes regularity on amorphous substrates and c-axis oriented group III-nitride films can be grown on the MLG buffer layers. It was also found that an insertion of AlN interlayers dramatically improves the phase purity and leads to formation of high quality wurtzite GaN. With the help of thermally oxidized AlN layers, GaN films grown on AlOx/AlN/MLG/SiO_2 showed Ga-polar. In-situ and ex-situ strain measurements of GaN grown on graphene showed that a small amount of strain is accumulated on GaN films. Because of the two-dimensionality of graphene, most of the strain that is generated by the lattice mismatch between MLG and nitrides is absorbed on the topmost layer of the MLG and a small amount of strain remains in the GaN films. Group III-nitride LEDs were grown successfully on amorphous SiO_2 substrates with MLG buffer layers. The LEDs exhibited clear EL emissions and the color of the LED changed from blue to red when the growth temperature of the MQWs was reduced.

The author developed the growth process of high quality group III nitride films on amorphous substrate at low growth temperature. The author extracts the following essentials for obtaining high-quality group III nitride crystalline films on amorphous substrates from these results: use of two dimensional MLG buffer layers, formation of abrupt interfaces between

group III nitrides and MLG, and polarity control of the GaN films.

By demonstrating that full-color LEDs can be fabricated on amorphous substrates, we suggest that since sputtering is very frequently used in the liquid crystal display industry, it is an established process that could be adapted to fabricate large-area inorganic LED displays on glass substrates. It should also be noted that state-of-the-art technology in the glass industry can offer roll-to-roll processing of flexible glass foils. The combination of these techniques can lead to the development of large-area flexible inorganic devices in the future.

List of the contents

Chapter 1

Introduction and Background

1.1 Group III-nitrides

Over the past two decades, group III-nitrides, such as AlN, GaN, InN and their alloys, have attracted considerable attention owing to their wide−range of direct band gap, physical stability and chemical stability. The wide range band gap makes the group III-nitrides ideal materials for optical devices operating in the near-infrared (NIR) to ultraviolet (UV) spectral region. The bandgap varies from 0.65 eV for indium nitride (InN), 3.40 eV for gallium nitride (GaN), to 6.2 eV for aluminium nitride (A1N) (Figure 1-1) [1.1–1.6]. Such a wide range band gap allows the group III-nitrides to have a broad range of applications in optoelectronic devices, such as light emitting diodes (LED), laser diodes (LD), and solar cells. Therefore, research efforts in this field have made rapid progress toward material growth and device fabrication [1.7–1.12].

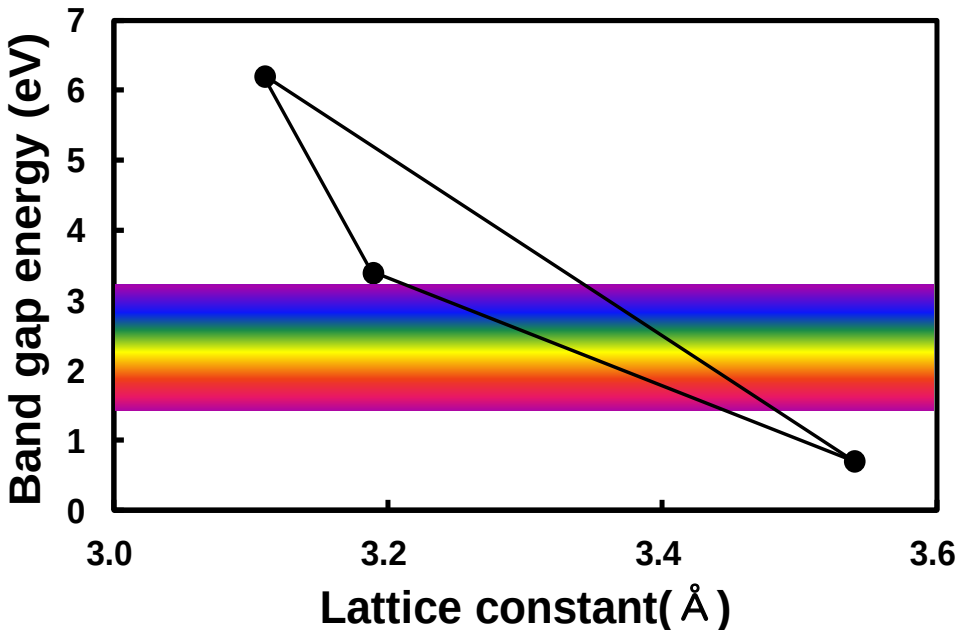

Figure 1-1 Band gap of group III-nitrides as a function of their lattice constants.

In addition, group III-nitrides are thermally, mechanically and chemically stable materials compared to conventional semiconductors, such as Si and GaAs [1.13]. In particular, the good thermal stability is due to the high bonding energy. Therefore, group III-nitrides electronic devices are capable of operating at high temperatures and in harsh environments.

Group III-nitrides can be grown either in the stable wurtzite (hexagonal) phase or metastable zincblende (cubic) phase depending on the growth conditions [1.14]. The wurtzite structures have hexagonal unit cells, with two lattice constants a and c, whereas the zincblende structures have cubic unit cells with equal lattice constants in the three perpendicular directions (Figure 1-2). AlN, GaN and InN have different lattice constants and band gaps owing to differences in ionic radii (i.e. Al^{3+}: 0.39 Å, Ga^{3+}: 0.47 Å, In^{3+}: 0.79 Å). Table 1-1 lists the lattice constants and band gap of group III-nitrides [1.15].

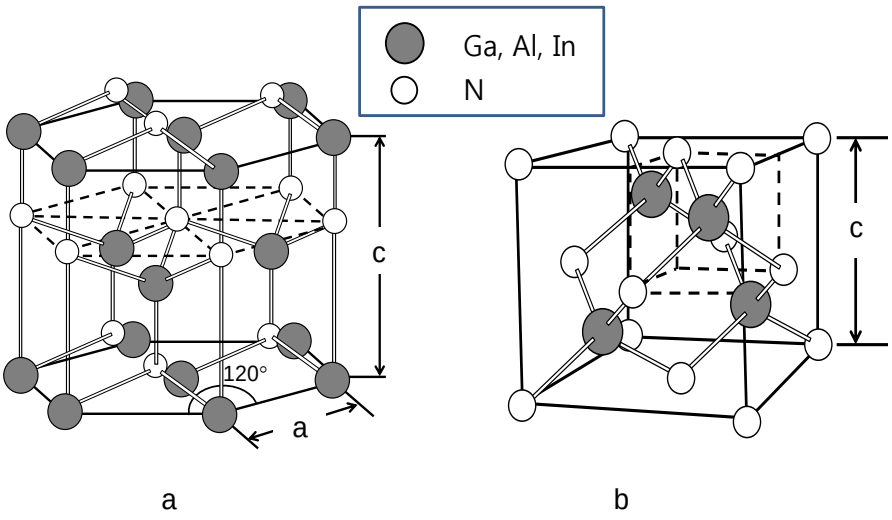

Figure 1-2 Atom arrangement in (a) wurtzite (hexagonal) and (b) zincblende (cubic) structures.

	AlN		GaN		InN	
	wurtzite	zincblende	wurtzite	zincblende	wurtzite	zincblende
a (Å)	3.11	4.38	3.19	4.50	3.54	4.98
c (Å)	4.98		5.18		5.71	
Energy gap (eV)	6.00	5.10	3.39	3.20	0.70	0.56

Table 1-1 Lattice constants and band gaps of AlN, GaN and InN [1.15].

Because group III-nitrides do not have inversion symmetry, the wurtzite group III-nitrides have polar axes. The most common growth direction of nitride is the <0001> direction, which causes polarity along the <0001> direction. The bulk and surface properties mainly depend on which are faced by nitrogen or metal atoms. The atoms are stacked in bilayers consisting of two close hexagonal layers, one with cations and the other with anions, so that the bilayers can form polar faces. Ga-polarity means that Ga is placed on the top position of the [0001] bilayers, whereas N-polarity means that nitrogen is placed on the top position of the [0001] bilayers.

Ga-polarity does not mean Ga-terminated, as shown in Figure 1-3. Termination should only be used to describe a surface property. Note that the polarity of [0001] differs from that of the [000 $\bar{1}$] direction.

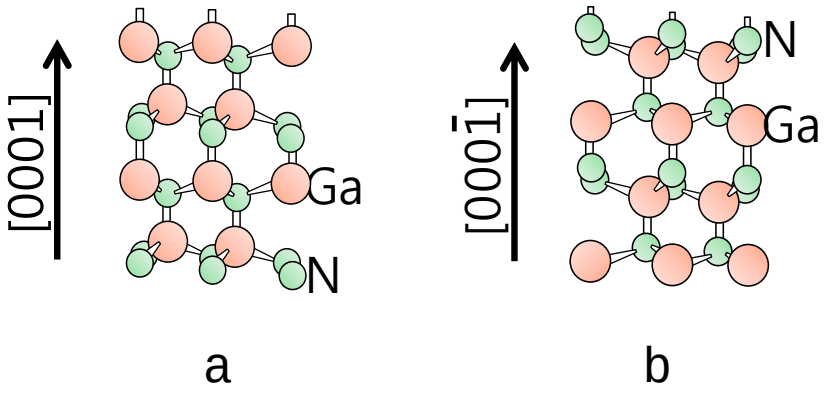

Figure 1-3 Polarity of wurtzite GaN (a) Ga-polarity and (b) N-polarity.

1.2 Growth technique for the heteroepitaxial growth of group III-nitride films

1.2.1 Heteroepitaxial growth of group III-nitride films

The best way to obtain high quality group III-nitride films is through the growth of nitride bulk substrates for homoepitaxy. On the other hand, there are considerable problems with the nitride bulk substrates for single crystal growth. These include excessive processing cost, prolonged process time and small substrate size. These issues have led to the use of foreign substrates for growing group III-nitride heteroepitaxially. Therefore, obtaining a suitable

substrate for the heteroepitaxial growth of III-nitride is critical in the development of nitride-based devices. To date, sapphire is the most commonly used substrate for nitride growth owing to its hexagonal symmetry, ease of surface cleaning, and high temperature stability (~1000 °C). Nevertheless, the use of sapphire could lead to large lattice mismatches and differences in the thermal expansion coefficients between the group III-nitrides and sapphire substrates. For example, the lattice mismatch between sapphire and GaN film is approximately 16%, as shown in Figure 1-4. The thermal expansion coefficient between sapphire and GaN film is approximately 26–34% [1.16]. These two phenomena generate strain and stress in group III-nitride films, which may cause problems, such as cracking of the substrate and group III-nitride films, and increase in the dislocation density. Moreover, the use of sapphire often restricts the application of GaN-based devices because of the limited availability of large-scale sapphire substrates. Therefore, to replace the sapphire substrates, many studies have focused on the development of new substrates, such as amorphous SiO_2, metal foils, and other oxide crystals [1.17–1.21].

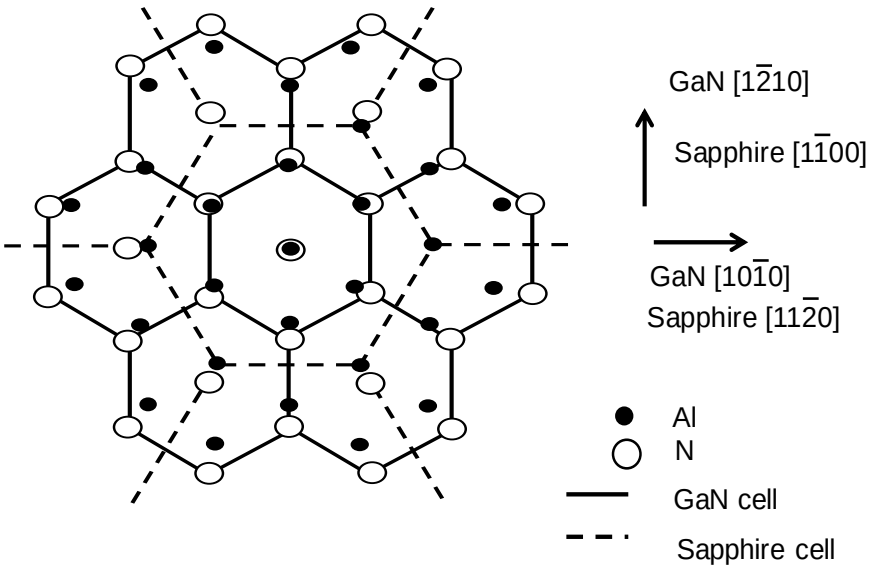

Figure 1-4 Lattice mismatch between sapphire and GaN film.

1.2.2 Metalorganic chemical vapour deposition (MOCVD)

Metalorganic chemical vapour deposition (MOCVD) uses the pyrolysis of vapour-phase mixtures of various chemical precursors in forming thin films of various materials [1.22]. The growth of group III-nitride films with the MOCVD process generally uses vapour phase mixtures of group III metalorganic and group V sources in a carrier gas. The carrier gas is typically purified H_2 or N_2. Growth is carried out in an open-tube process chamber as shown in Figure 1-5. The MOCVD process involves series of complicated gas phase and surface reactions.

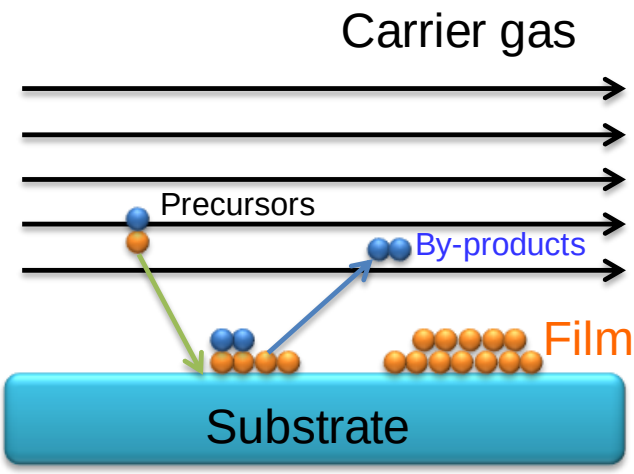

Figure 1-5 Schematic diagram of the chemical vapour deposition process.

The growth of group III-nitride films by MOCVD requires a minimum deposition temperature to ensures the mobility of surface species during the growth of group III-nitride films. Trimethylgallium (TMG), the conventional MOCVD precursor adopted for GaN growth, begins to pyrolyze at temperatures higher than 450 °C. GaN films with the best electrical and optical properties are grown at 1050 °C [1.23].

1.2.3 Pulsed sputtering deposition (PSD)

PSD is a physical deposition method that uses pulsed plasma as the excitation source. This technique is based on the ion bombardment of a source target plate, which is bombarded by energetic ions generated in glow discharge plasma. The bombardment process causes the sputtering of target atoms, which may then condense on the substrate as film (Figure 1-6). The growth of group III-nitride films is attributed to the high kinetic energies that facilitate the

surface migration of the film precursors over the substrate surface. Therefore, this technique can be classified as a physical vapour deposition technique [1.24].

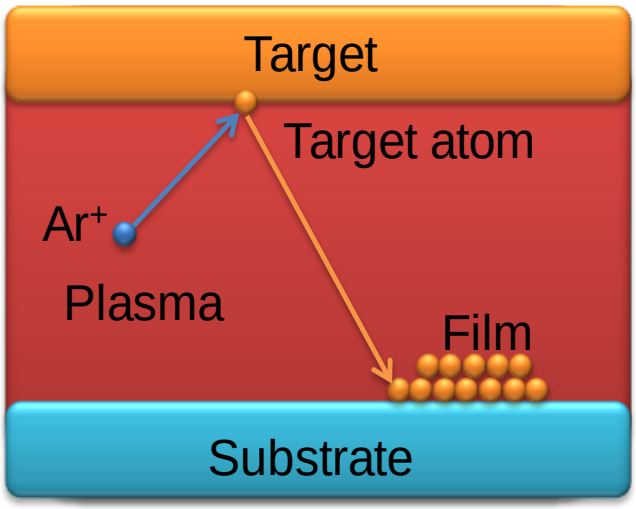

Figure 1-6 Schematic diagram of the sputtering deposition.

Recent progress in low-temperature epitaxial growth techniques based on pulsed sputtering deposition (PSD) has enabled to grow group III-nitrides, even at room temperature [1.25–1.26]. The successful decrease in the growth temperatures in PSD has been attributed to the high kinetic energy and the pulsed supply of the group III atoms, which facilitates in the surface migration of the film precursors at the substrate surfaces [1.27]. The use of pulsed supply of group III atoms enhances the migration at the substrate surfaces, which in turn leads to the formation of epitaxial films with high crystalline quality.

1.3 Growth of group III-nitride on amorphous glass substrate

Among the many novel substrate candidates for group III-nitride films, flat glass is a promising substrate material because of its large-area scalability and low manufacturing cost. Furthermore, glass substrates are suitable materials for flat light sources including the backlight for liquid crystal displays (LCDs) because of their low cost, versatility and transparency. Despite the advantages of glass substrates, GaN films on glass have not yet been used in practice because of the following two serious problems.

The first problem is the low operating temperature of glass: the softening temperature of general glass materials is less than 500°C. The substrate temperature for GaN growth is normally higher than 1000°C in conventional metalorganic chemical vapour deposition (MOCVD). Therefore, glass cannot be used as a substrate to grow GaN by ordinary MOCVD. Y. J. Hong *et al.* proposed GaN growth on soda lime glass by the heteroepitaxial coating of GaN on ZnO nanorods using a local microheating method as shown in Figure 1-7 [1.28]. Y. J. Hong *et al.* introduced molybdenum (Mo) microheater arrays consisting of a number of heater units connected in parallel and series between two common electrodes. Using this growth method, GaN/ZnO nanorod heterostructures were produced with single crystallinity with clean and abrupt interfaces. On the other hand, microbridge heaters need to be installed on glass substrates to implement the growth method, which limits the use of glass as substrate material.

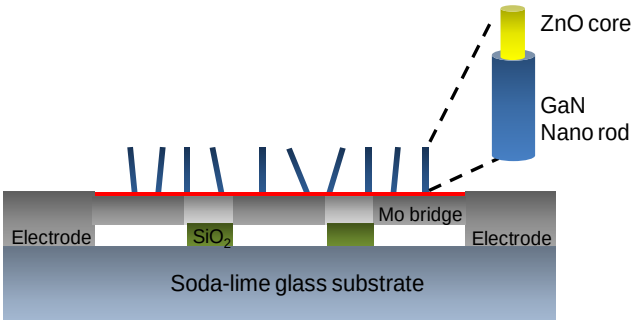

Figure 1-7 Schematic diagram of the fabrication process for obtaining GaN/ZnO coaxial nanorod heterostructures on glass substrates using the microheating method [1.28].

The second problem with the glass substrates is the amorphous nature of glass, which leads to poor crystalline quality of GaN films grown on glass. Despite the advantages of glass substrates, growing group III-nitrides directly on amorphous glass substrates has been hampered by the lack of an epitaxial relation. Group III-nitrides grown on glass have random orientations because of the amorphous property of glass. To solve this problem, Jun Hee Choi *et al.* fabricated nearly single-crystal GaN pyramid arrays on amorphous fused-silica glass substrates [1.29]. J. H. Choi *et al.* developed a process that uses a 'pre-orienting layer' and SiO_2 mask layers to achieve nearly single-crystal GaN pyramid arrays on amorphous fused silica glass substrates. J. H. Choi *et al.* used vacuum-evaporated, thin-film titanium grown on amorphous fused silica glass substrates and low-temperature GaN as the pre-orienting and nucleation layers, respectively. They chose titanium because it has the same hexagonal crystal lattice structure as wurtzite GaN and a relatively small lattice mismatch. The sample structure of this group consisted of high temperature (HT)-GaN/hole-patterned SiO_2/low temperature (LT)-GaN/Ti/fused silica glass, as shown in Figure 1-8. Even with this process, HT-GaN was

grown at approximately 1040 °C by MOCVD. Conventional glass cannot tolerate such a high growth temperature.

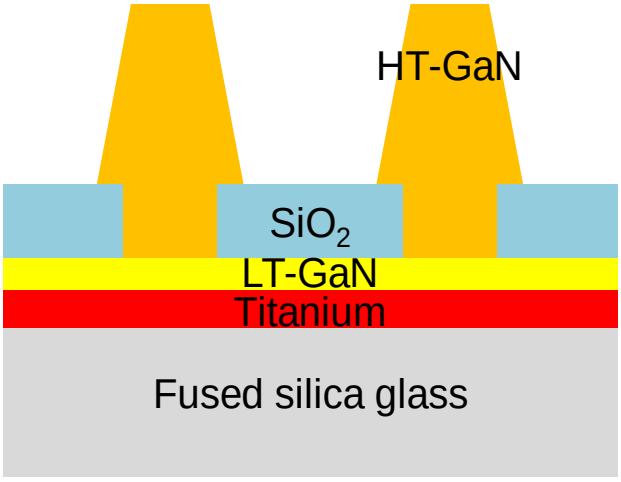

Figure 1-8 Schematic diagram of GaN grown on fused silica glass [1.29].

As described above, it is impossible to use glass as a group III-nitride substrate because of its softening temperature and amorphous property.

1.4 Growth of group III-nitride with a graphene layer

1.4.1 Graphene

Graphene is a two-dimensional material, which is based on hexagonally arranged carbon atoms. Graphene is held together with sp^2 bonds between the carbon atoms separated by a distance of approximately 1.4 Å with strong in-plane bonding and a-lattice parameter of graphene is 2.85 Å, as shown in Figure 1-9 [1.30]. Graphene is a promising material for device

applications because of its excellent properties, which is often also valid for bilayer and few-layer graphene. Graphene is the base of graphite, which is constructed from stacked one-atom thick layers. The interlayers are held mainly by weak van-der Waals forces compared with the strong in-plane bonding. Therefore, glass substrates can be a proper solution by introducing crystalline graphene buffer layers between the amorphous glass substrate and GaN films.

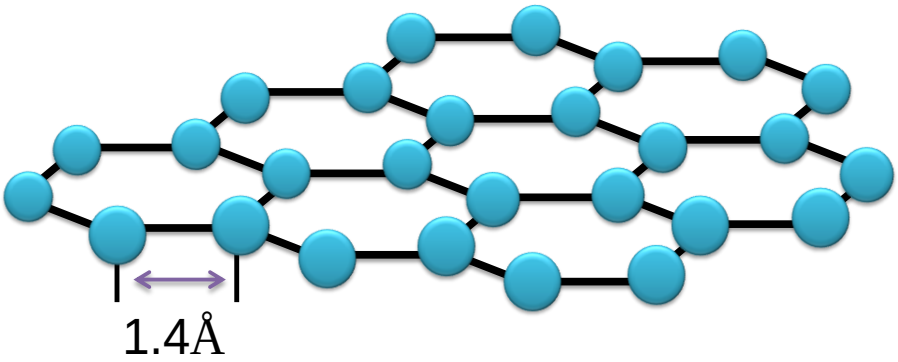

Figure 1-9 Schematic diagram of a graphene layer.

In 2004, Konstantin Novoselov and Andre Geim discovered a new method to produce only one-atom thick high quality graphene, through mechanical exfoliation with scotch tape from highly oriented pyrolytic graphite (HOPG). Their method suggests ways to produce pure graphene under experimental conditions [1.31]. On the other hand, the exfoliation method limits the size and amount of graphene. Many groups have developed a variety of methods to overcome these limitations, such as the reduction of graphene oxide [1.32], epitaxial graphene growth on SiC substrates [1.33], and graphene growth on metal substrates [1.34–1.39]. Among these methods, the chemical vapour deposition of graphene has the advantage of being able to

provide large-size and relatively uniform graphene films, e.g. 30 in roll-based graphene films [1.40].

Although there are many concerns regarding the use of graphene as a conducting electrode for group III-nitride LEDs [1.41–43], it is less likely that graphene can be used as the interlayer or substrate for group III-nitride because the pristine graphene surface lacks chemical reactivity. Therefore, the use of graphene necessitates additional surface treatment.

1.4.2 GaN growth on graphene layers with ZnO nanowalls

Kunook Chung's group fabricated transferable GaN thin films and LEDs using graphene-layered sheets [1.44–1.45]. Oxygen plasma treatments were applied to a graphene surface and vertically aligned ZnO nanowalls were grown on the grapheme surfaces by MOCVD. GaN islands can be grown along the graphene step edges and oxygen plasma treatment can produce graphene step edges as shown in Figure 1-10. The graphene step edges generated by oxygen-plasma lead to the formation of high density vertically aligned ZnO nanowalls. Low-temperature (LT, 540–600 °C) GaN films grow on the ZnO nanowalls by lateral overgrowth. Subsequently, high temperature GaN films were grown at 1080-1100 °C.

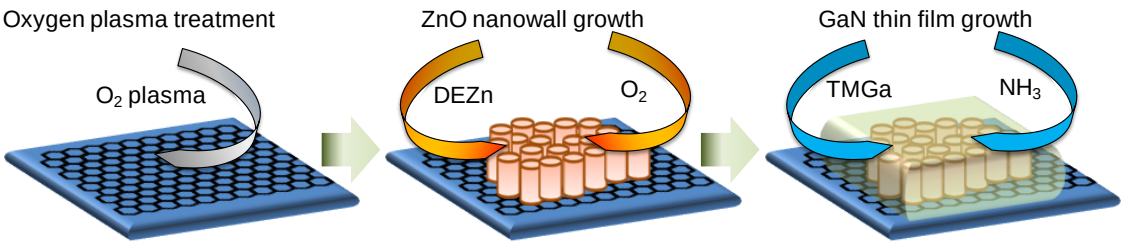

Figure 1-10 Schematic diagrams of the fabrication processes for GaN [1.44].

The oxygen plasma-treated graphene and the complex semiconductor interface of such an approach certainly have significant trap centres for carriers that degrade the performance. Therefore, the ability to grow group III-nitrides directly on the graphene with minimal interface defects is essential for high performance devices.

The height of the ZnO nanowalls is 200–400nm and the thickness of LT GaN has to be more than the height of the ZnO nanowalls. When the LT GaN thickness is smaller than the height of the ZnO nano wall, unintended interactions can take place between the ZnO nanowall and GaN at high growth temperatures. Compared with the conventional thickness of the LT GaN buffer layer (less than 100 nm), the thickness of LT GaN in this method is too high to obtain high quality GaN. Moreover, the growth temperature of GaN is greater than 1000°C, which is too high to grow group III- nitride on glass substrates.

1.4.3 GaN growth on functionalized epitaxial graphene

Neeraj Nepal's group reported the growth of epitaxial GaN films by MOCVD on functionalized epitaxial grapheme (EG) using a thin conformal AlN nucleation layer, as shown in Figure 1-11 [1.46]. Growing group III-nitrides directly on graphene is challenging because there are no dangling bonds on the surface of graphene to promote bonding with foreign atoms. As a result, functionalization methods were used to modify the graphene surface promote bond formation and create pristine graphene surfaces without any surface damage.

EG was grown on 4° 4H-SiC samples using the Si sublimation method. EG/SiC was patterned with SiN_x deposited by plasma enhanced CVD. This patterned EG was functionalized

using pulses of XeF_2 plasma to form approximately 6–7% ‘semi-ionic’ C–F bonds. Atomic layer epitaxy (ALE) enables the growth of thin (~11 nm) and uniform AlN layers at low temperature (280 °C), which is required to preserve the essential fluorine functional groups. GaN was then grown by MOCVD.

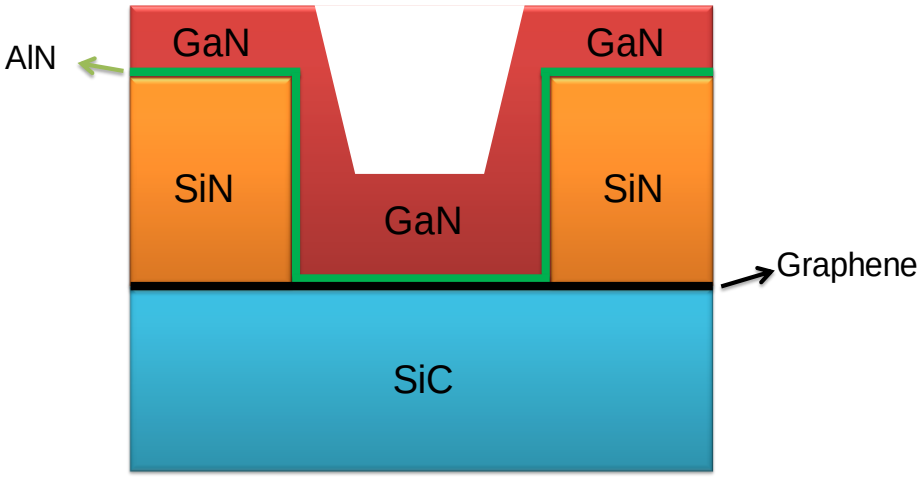

Figure 1-11 Schematic diagram showing GaN/AlN/graphene/SiC layers [1.46].

The functionalization has been applied to EG layers grown on SiC substrates. This method cannot be used for growing crystalline graphene buffer layers for glass substrates.

1.4.4 MOVPE growth of semi-polar group III-nitride on CVD graphene

Priti Gupta's group reported the growth of group III-nitride semiconductor layers on graphene grown by CVD [1.47]. GaN, AlGaN alloys and InN layers were grown by metal organic vapour phase epitaxy (MOVPE) using an AlN nucleation and a buffer layer.

The lack of chemical reactivity of the graphene surface interrupted the flat and smooth GaN film surface growth. The direct growth of GaN on graphene surfaces induced a plethora of Ga droplets and a mass of facetted GaN. Therefore AlN layers were used as a buffer for GaN growth because of the higher sticking coefficient and much shorter diffusion length of Al adatoms on the surface [1.48]. The deposition of low-temperature (800 °C) AlN provides a conformal nucleation layer on which an AlN buffer layer can be grown. Subsequently, GaN is grown at 1040 °C on an AlN buffer layer. Figure 1-12 shows the structure of the GaN grown on graphene with an AlN buffer and a nucleation layer.

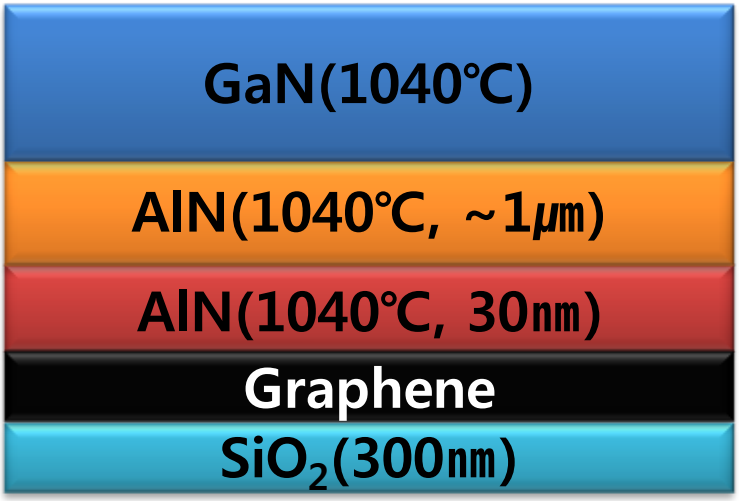

Figure 1-12 Structure of GaN grown on graphene with an AlN layer [1.47].

This group succeeded in growing semipolar group III-nitrides. Semipolar oriented layers can be obtained by controlling the growth conditions. Other groups ([1.43-1.45]) reported the growth of c-axis orientated ((0001) orientated) wurtzite group III-nitride films. Although AlN buffer and nucleation layers are inserted between GaN and graphene, GaN showed poor surface

morphology and crystal quality. Moreover, the growth temperatures (800~1040°C) are higher than the process temperature of glass. Therefore, this method cannot be used with a glass substrate.

1.4.5 One-step graphene coating of heteroepitaxial GaN films

Jae-Kyung Choi's group reported the use of graphene as the coating layer in the one-step growth of heteroepitaxial GaN films on sapphire substrates in a MOCVD reactor, as shown in Figure 1-13 [1.49]. With increasing graphene coating layer thickness, the structural and optical properties of one-step grown GaN films approach those of GaN films grown with the conventional two-step growth method. The ultrathin graphene layers greatly improve the wetting between the sapphire surface and the GaN film.

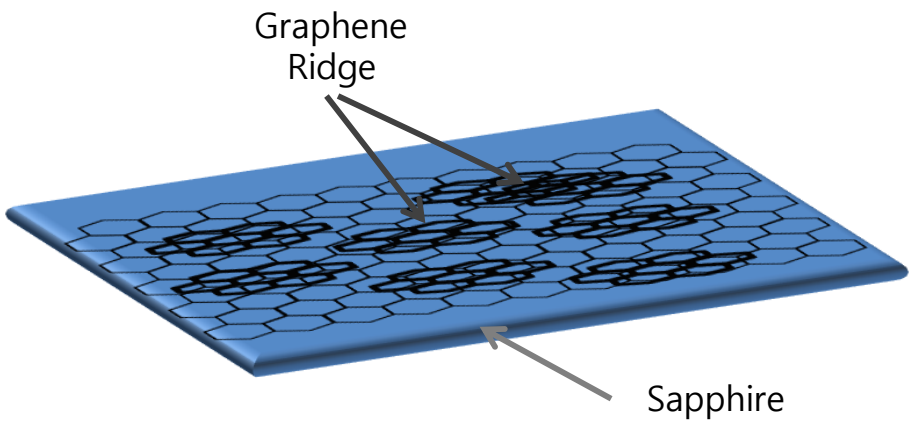

Figure 1-13 Scheme of the one-step growth of epitaxial GaN films [1.49].

Epitaxial GaN films cannot be grown on pristine graphene layers because of their chemical stability. GaN films on graphene coating layer have epitaxial relation with the underlying sapphire substrate. Therefore, this method is unsuitable for GaN growth on an amorphous substrate.

1.5 Growth of group III-nitride with hexagonal boron nitride (h-BN)

Y. Kobayashi's group reported that they used single-crystal h-BN as the buffer and release layer for growing of group III-nitride films with MOVPE [1.50]. GaN directly grown on the h-BN buffer layer had a rough and irregular island-shaped surface morphology, and was polycrystalline. XRD measurement revealed that GaN $10\bar{1}0$, 0002, and $10\bar{1}1$ diffractions was observed, indicating the crystal structure of the GaN layer was polycrystalline. This polycrystalline GaN was also observed in the case of polycrystalline h-BN buffer layers [1.51]. The insertion of an AlN or AlGaN layer between the h-BN layer and GaN layer improves the surface morphology and crystalline quality of nitride films. The single-crystal h-BN layer with atomically flat surface enables the growth of AlGaN/GaN heterostructures and InGaN-based multiple quantum wells (MQWs) and LEDs structures and the release of these structures from the host sapphire substrates and their transfer to foreign substrates.

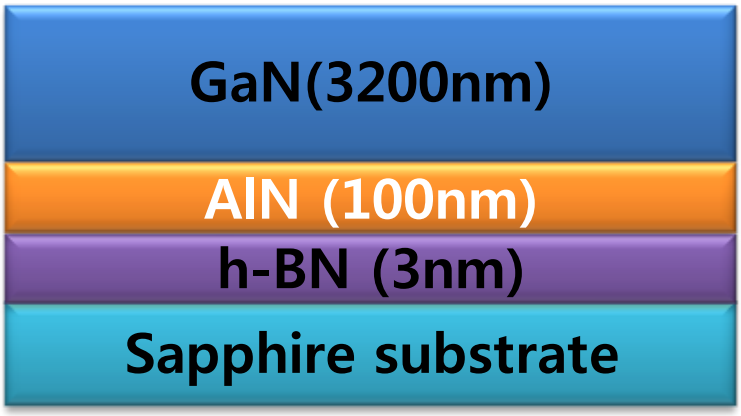

Figure 1-15 Structure of GaN grown on sapphire with h-BN layer [1.50].

Y. Kobayashi's group used the MOVPE technique to grow group III-nitride films. The growth temperature of the films had a lower limit that was higher than the glass transition temperature. Hence, this technique cannot be applied to glass substrates.

For LEDs driven by constant current source, the light output drops with increasing temperature. This means that thermal managements are needed and high thermal conductivity is one of the important characteristics of the LED. On the other hand, the room-temperature, 360 $Wm^{-1}K^{-1}$ thermal conductivity of h-BN is lower than the ≥2000 $Wm^{-1}K^{-1}$ thermal conductivity of multi-layer grapheme (MLG) [1.52–1.54]. Therefore, during LED operation, h-BN accumulates more heat than MLG and increases the device temperature.

The shortcoming of this method is the use of single crystal h-BN. Polycrystalline GaN films grow on polycrystalline h-BN films with random in-plane orientations, which are unsuitable for growing LED structures. To date, the grown single crystal h-BNs are approximately several square centimetres, which limits the use of single crystal h-BN [1.55].

1.6 Purpose of this study

Group III-nitrides (AlN, GaN and InN) have been studied extensively because of their excellent properties, such as the wide-range band gap energy (0.65–6.2 eV), direct transition band structure, high breakdown field and high thermal stability. Many studies on the heteroepitaxial growth of group III-nitrides have been performed. Considerable research efforts have contributed to the successful epitaxial growth of group III-nitrides with high crystalline quality on sapphire substrates. On the other hand, sapphire substrates limit the performance of nitride devices because of the scarcity of large crystals and the high fabrication cost. Glass is an effective substrate for future LEDs because of its scalability and low cost. GaN films on glass substrates, however, have not been used in practice because of glass amorphous nature and low softening temperature. The epitaxial growth of high quality group III-nitride films on glass substrates has not been achieved. The introduction of a crystalline buffer layer and low temperature group III-nitride growth techniques may solve the glass substrate problems. Several groups have reported the growth of group III-nitride on amorphous substrates using an extra heating apparatus, local pyramid arrays, and graphene layers. On the other hand, they did not simultaneously solve all the problems, e.g. low growth temperature and amorphous nature of the glass substrate which has limited the use of amorphous glass substrates to date.

The motivation for this study was to fabricate high quality group III-nitride films on amorphous substrates and assess their application to LEDs. PSD techniques were used to grow group III-nitrides on amorphous SiO_2 substrates with MLG as the crystalline buffer layer and LED structures were fabricated.

The aims of this study were the follow.

1. Growth of group III-nitrides on amorphous substrates with MLG buffer layers by PSD.
2. Characterization of the group III-nitride films grown on the MLG buffer layers.
3. Fabrication of a LED structure that covers the entire visible light region from blue to red on amorphous SiO_2 substrates with MLG buffer layers.

In chapter 1, I provide a brief introduction to the concepts relevant to the study of the heteroepitaxial growth of group III-nitrides. In this chapter the growth of group III- nitride films on several substrates is briefly discussed.

In chapter 2, I present the results for group III-nitrides grown on amorphous SiO_2 substrates with MLG buffer layers by PSD. The growth of *c*-axis oriented GaN and AlN films is verified. The direct growth of GaN on MLG buffer layers results in the coexistence of both zincblende and wurtzite phases of GaN. The insertion of AlN interlayers between the MLG buffer layers and GaN films improves dramatically the phase purity of wurtzite GaN in the films. The use of AlN interlayers with and without surface oxidization, leads to the formation of Ga- and N-polar GaN films, respectively.

In chapter 3, I discuss the strain generation in the GaN films, which are grown by PSD. An *In- situ* strain measurement system for group III-nitride films grown by PSD, which is based on measuring the curvature induced in the substrate by the strained film, was developed. In this study, both In- situ and ex- situ strain measurements were performed. As a result, the change in beam separation during GaN growth on SiO_2 with MLG buffer layers was quite small, indicating small strain in the GaN films. Because of the two-dimensionality of graphene, the

topmost layer of MLG was extended to have a longer lattice constant close to that of GaN.

Chapter 4 covers the fabrication of the LED structure on amorphous SiO_2 substrates with MLG buffer layers. The LEDs fabricated on the GaN films with MLG buffer layers exhibited clear EL emissions from blue to red. The colour of LEDs on SiO_2 with MLG buffer layers was adjusted by changing the In compositions in the InGaN wells of MQWs.

In chapter 5, I summarize the study results and discuss future prospects.

The results suggest that MLG buffer layers and PSD techniques are promising for the manufacturing large-area and flexible light emitting devices on amorphous substrates.

References

[1.1] F. A. Ponce, and D. P. Bour, Nature **386**, 531 (1997).

[1.2] S. Nakamura, Science **281**, 956 (1998).

[1.3] E. Silveira, J.E. Freitas, B. Schujman, and L.J. Schpwalter, J. Cryst. Growth **310**, 4007 (2008).

[1.4] J. Wu, W. Walukiewicz, K.M. Yu, J.W. Ager III, E.E. Haller, Hai Lu, W. J. Schaff, Y. Saito, and Y. Nanishi, Appl. Phys. Lett. **80**, 3967 (2002).

[1.5] T. Suzuki, H. Yaguchi, H. Okumura, Y. Ishida, and S. Yoshida, Jpn. J. Appl. Phys. **39**, L497 (2000).

[1.6] J. Schörmann, D.J. As, K. Lischka, P. Schley, R. Goldhahn, S.F. Li, W. Löffler, M. Hetterich, and H. Kalt, Appl. Phys. Lett. **89**, 261903 (2006).

[1.7] M. Ueno, M. Yoshida, A. Onodera, O. Shimomura, and K. Takemura, Phys. Rev. B **49**, 14 (1994).

[1.8] H. Morkoc, S. Strite, G. B. Gao, M. E. Lin, B. Sverdlov, and M. Burns, J. Appl. Phys. **76**, 1363 (1994).

[1.9] S. Nakamura, T. Mukai, and M. Senoh, Appl. Phys. Lett. **64**, 1687 (1994).

[1.10] M. Asif Khan, M. S. Shur, J. N. Kuznia, Q. Chen, and J. Burn, W. Scha Appl. Phys. Lett. **66**, 1083 (1995).

[1.11] S. N. Mohammad, Z.-F. Fan, A. Salvador, O. Aktas, A. E. Botchkarev, W. Kim. and H. Morkoc, Appl. Phys. Lett. **69**, 1420 (1996).

[1.12] S. Nakamura, M. Senoh, N. Iwasa. and S. Nagahama, Jpn. J. Appl. Phys. **34**, L797 (1995).

[1.13] L. Sorba, S. Yildirim, M. Lazzarino, A. Franciosi, D. Chiola, and F. Beltram, Appl. Phys. Lett. **69**, 1927 (1996).

[1.14] J. W. Orton. and C. T. Foxon, Rep. Prog. Phys. **61**, 1 (1998).

[1.15] O. Ambacher, J. Phys. D: Appl. Phys. **31**, 2653 (1998).

[1.16] H. Amano, K. Hiramatsu, and I. Akasaki, J. Appl. Phys. **27**, L1384 (1988).

[1.17] D. P. Bour, N. M. Nickel, C. G. Van de Walle, M. S. Kneissl, B. S. Krusor, P. Mei, and N. M. Johnson, Appl. Phys. Lett. **76**, 2182 (2000).

[1.18] S. Guha, and N. A. Bojarczuk, Appl. Phys. Lett. **72**, 415 (1998).

[1.19] A. Kobayashi, H. Fujioka, J. Ohta, and M. Oshima, Jpn. J. Appl. Phys. **43**, L53 (2004).

[1.20] J. Ohta, H. Fujioka, and M. Oshima, Appl. Phys. Lett. **83**, 3060 (2003).

[1.21] S. Inoue, K. Okamoto, T. Nakano, J. Ohta, and H. Fujioka, Appl. Phys. Lett. **91**, 201920 (2007).

[1.22] P. Gibart, Rep. Prog. Phys. **67**, 667 (2004).

[1.23] R. Niebuhr, K. Bachem, K. Dombrowski, M. Maier, W. Pletschen. and U. Kaufmann, J. Electron. Mater. **24**, 1531 (1995)

[1.24] P.J. Kelly, and R.D. Arnell, Vacuum **56**, 159 (2000).

[1.25] K. Sato, J. Ohta, S. Inoue, A. Kobayashi, and H. Fujioka, Appl. Phys. Express **2**, 011003 (2009).

[1.26] K. Okubo, A. Kobayashi, J. Ohta, M. Oshima, and H. Fujioka, Appl. Phys. Lett. **102**, 022103 (2013).

[1.27] A. K. Geim, and K. S. Novoselov, Nat. Mater. **6**, 183 (2007).

[1.28] Y. J. Hong, Y. Kim, J. Jeon, M. Kim, J. H. Choi, C.W. Baik, S. I. Kim, S. S. Park, J.M. Kim, and G. Yi, Nat. Nanotech. **22**, 205602 (2011).

[1.29] J. H. Choi, A. Zoulkarneev, S. I. Kim, C. W. Baik, M. H. Yang, S. S. Park, H. Suh, U. J. Kim, H. B. Son, J. S. Lee, M. Kim, J. M. Kim. and K. Kim, Nat. Photonics **5**, 763 (2011).

[1.30] Z. Chen, R. S. Qhalid Fareed, M. Gaevski, V. Adivarahan, J. W. Yang, Asif Khan, J. Mei and F. A. Ponce, Appl. Phys. Lett. **89**, 081905 (2006).

[1.31] S. V. Morozov, K. S. Novoselov, F. Schedin, D. Jiang, A. A. Firsov, and A. K. Geim, Phys. Rev. B **72**, 201401 (2005).

[1.32] S. Park, and R.S. Ruoff, Nat. Nanotech. **4**, 217 (2009).

[1.33] C. Berger, Z. Song, X. Li, X. Wu, N. Brown, C. Naud, D. Mayou, T. Li, J. Hass, A. N. Marchenkov, E. H. Conrad, P. N. First, and W. A. de Heer, Science **312**, 1991 (2006).

[1.34] K. V. Emtsev, A. Bostwick, K. Horn, J. Jobst, G. L. Kellogg, L. Ley, J. L. McChesney, T. Ohta, S. A. Reshanov, J. Rohrl, E. Rotenberg, A. K. Schmid, D. Waldmann, H. B. Weber, and T. Seyller, Nat. Mater. **8** (3), 203 (2009).

[1.35] Q. Yu, J. Lian, S. Siriponglert, H. Li, Y. P. Chen, and S. S.Pei, Appl. Phys. Lett. **93**, 113103 (2008).

[1.36] A. Reina, X. Jia, J. Ho, D. Nezich, H. Son, V. Bulovic,M. S. Dresselhaus, and J. Kong, Nano Lett. **9**, 30 (2009).

[1.37] P.W. Sutter, J. I. Flege, and E. A. Sutter, Nat. Mater. **7**, 406 (2008).

[1.38] K. S. Kim, Y. Zhao, H. Jang, S. Y. Lee, J. M. Kim, K. S. Kim, J. H. Ahn, P. Kim, J. Y. Choi,and B. H. Hong, Nature **457**, 706 (2009).

[1.39] X. S. Li, W. W. Cai, J.H. An, S. Kim, J. Nah, D. X. Yang, R. D. Piner, A. Velamakanni, I. Jung, E. Tutuc, S. K. Banerjee, L. Colombo, and R. S. Ruoff, Science **324**, 1312 (2009).

[1.40] S. Bae1, H. Kim, Y. Lee, X. Xu, J. Park, Y. Zheng, J. Balakrishnan, T. Lei, H. R. Kim, Y. I. Song, Y. Kim, K. S. Kim, B. O¨ zyilmaz, J. Ahn, B. H. Hong, and S. Iijima1, Nat. Nanotech. **5**, 574 (2010).

[1.41] G. Jo, M.Choe, C. Y.Cho, J. H. Kim,and W. Park, Nat. Nanotech. **21**, 175201 (2010).

[1.42] B. J. Kim, M. A. Mastro, J. Hite, C. R. Eddy, and J. Kim, Opt. Express **18**, 23030 (2010).

[1.43] J. M. Lee, H. Y. Jeong, K. J. Choi, and W. I. Park, Appl. Phys. Lett. **99**, 041115 (2011)

[1.44] K. Chung, C. LEE, and G. Yi, Science **330**, 655 (2009)

[1.45] K. Chung, S. I. Park, H. Baek, J. Chung, and G. Yi, NPG Asia Mater. **4**, e24 (2012)

[1.46] N. Nepal, V. D Wheeler, T. J Anderson, F. J Kub, M. A Mastro, R. L Myers-Ward, S. B Qadri, J. A Freitas, S. C Hernandez, L. O Nyakiti, S. G Walton, K. Gaskill, and C. R Eddy Jr., Appl. Phys. Express **6,** 061003 (2013)

[1.47] P. Gupta, A. A. Rahman, N. Hatui, M. R. Gokhale, M. M. Deshmukh, and A. Bhattacharya, J. Cryst. Growth **372**, 105 (2013).

[1.48] S. R-Clur, O. Briot, J. L. Rouvière, B. Gil, and R. L. Aulombard, Mater. Sci. Eng., B **B50**, 219 (1997).

[1.49] J. Choi, J. Huh, S. Kim, D. Moon, D. Yoon, K. Joo, J. Kwak, J. H. Chu, S. Y. Kim, K. Park, Y. Kim, and E. Yoon, Nat. Nanotech. **23**, 435603 (2012)

[1.50] Y. Kobayashi, K. Kumakura, T. Akasaka, and T. Makimoto, Nature, **484**, 223 (2012).

[1.51] J. Boo, C. Rohr, and W. Ho, J. Cryst. Growth **189/190**, 439 (1998).

[1.52] SI. Jo, M. T. Pettes, J. Kim, K. Watanabe, T. Taniguchi, Z. Yao, and L. Shi, Nano Lett. **13**, 550 (2013).

[1.53] S. Ghosh,W. Bao, D. L. Nika, S. Subrina, E. P. Pokatilov, C. N. Lau, and A. A. Balandin, Nat. Mater. **9**, 555 (2010).

[1.54] D. L. Nika, S. Ghosh, E. P. Pokatilov, and A. A. Balandin, Appl. Phys. Lett. **94**, 203103 (2009)

[1.55] L. Song, L. Ci, H. Lu, P. B. Sorokin, C. Jin, J. Ni, A. G. Kvashnin, D. G. Kvashnin, J. Lou, B. I. Yakobson, and P. M. Ajayan, Nano Lett. **10**, 3209 (2010).

Chapter 2

Structural control of GaN films

2.1 Introduction

GaN has been studied intensively because of its excellent properties, such as a wide range of band gap, direct transition band structure, high breakdown field, and high stability [2.1, 2.2]. These excellent properties make them suitable for optical devices, such as light emitting diodes (LED) and laser diodes, ranging from the ultraviolet to the infrared region [2.3, 2.4]. Despite the limitations imposed by the sapphire substrates, such as poor thermal conductivity, insulating properties, and unavailability of large-size wafers, GaN films are commonly grown on sapphire substrates. The shortcoming of sapphire substrates have hindered the potential of group III-nitrides and their wider application to large-area and flexible devices. To overcome these problems, many studies have attempted to use a range of substrate materials for growing GaN including metal, graphite, fused silica, and functional oxides [2.5-2.10]. Among these materials, glass is a promising substrate material because of its scalability and low cost [2.11]. On the other hand, GaN films on glass have not been put into practical use because of the following two serious problems. One problem is the amorphous nature of glass, which results in poor crystalline quality of GaN films grown on glass. To address this problem, crystalline buffer layers between the amorphous substrate and GaN films are introduced. Graphene is well suited for this purpose, because large-area multi-layer graphene (MLG) is available and is easily transferred onto foreign substrates. The other problem is the low softening temperature of glass.

Because the growth temperature of GaN films is normally higher than 1000 °C in conventional metalorganic chemical vapour deposition (MOCVD), it is difficult to use glass as substrate in MOCVD. Fortunately, recent progress in low-temperature epitaxial growth techniques based on pulsed sputtering deposition (PSD) has enabled to grow group III-nitrides even at room temperatures [2.12, 2.13]. The successful decrease in the growth temperatures in PSD has been attributed to the high kinetic energy and the pulsed supply of group III atoms, which assists the surface migration of the film precursors at the substrate surfaces. This important feature of PSD might allow the fabrication of nitride devices below the softening temperature of glass.

In this chapter, I discuss for the first time growth of GaN films on SiO_2 with MLG buffer layers by PSD and the structural investigations of GaN films

2.2 Experimental procedure

MLG buffer layers were grown by CVD and transferred to the SiO_2 surfaces. MLG layers were used as starting materials to grow group III-nitride films [2.14]. Thermally oxidized 100nm-thick SiO_2 / 525 μm-thick Si (100) was used as the substrate. Before the growth of GaN films, the MLG/ SiO_2/Si substrates were degassed at 600 °C for 30 min in vacuum. The growth of GaN and AlN films was performed using a PSD apparatus with a background pressure of 1.0×10^{-10} Torr. The growth temperatures of the films were set at 650-1050 °C. Sputtering of the Ga and Al targets was performed in a N_2/Ar gaseous ambient. The thickness of GaN and AlN was 600 nm and 50 nm, respectively. The structural properties of the GaN films were investigated by X-ray diffraction (XRD) using a Bruker D8 diffractometer, and electron

back-scattered diffraction (EBSD) using an Oxford Instruments INCA Crystal EBSD system attached to a field emission scanning electron microscope (JEOL JSM-6500F) operated at 20 kV. The phase purity of the GaN films was measured by scanning Kikuchi pattern identification using EBSD [2.15]. Wet chemical etching by a 1.8 M KOH solution was also performed to determine the polarity of the GaN films. The optical properties of the films were characterized by room-temperature photoluminescence (PL) using a He-Cd laser (λ=325 nm) as the excitation source.

2.3 GaN films growth on amorphous SiO_2 with MLG

To grow group III-nitride films on amorphous SiO_2 substrates, the MLG layers were introduced as crystalline buffer layers for growing group III-nitride films on amorphous substrate. GaN films (~ 1000 nm) were grown on SiO_2/Si(100) substrates with MLG buffer layers by PSD. Figure 2-1 shows a schematic diagram of the sample structure.

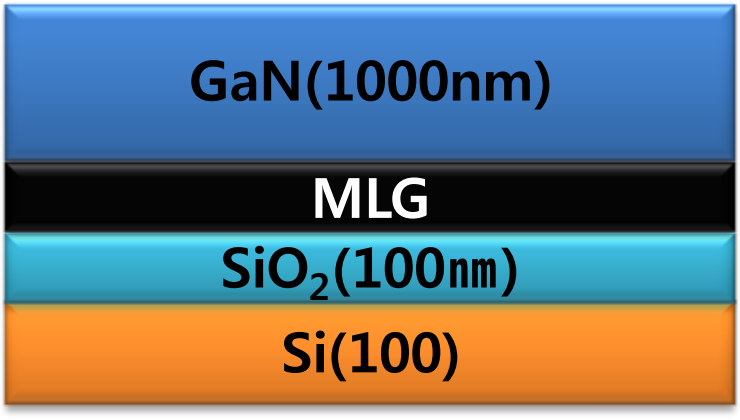

Figure 2-1 Schematic diagram of GaN grown on amorphous SiO_2 with MLG.

Figure 2-2 shows the XRD 2θ/ω curve of the GaN films grown at 750 °C with MLG buffer layers. XRD peaks were observed at approximately 34.5°, 69.1° and 72.9°. The peaks correspond to the diffractions from GaN 0002, Si 004, and GaN 0004, respectively. This suggests that the GaN films grown on amorphous SiO_2 with MLG have highly c-axis oriented structures.

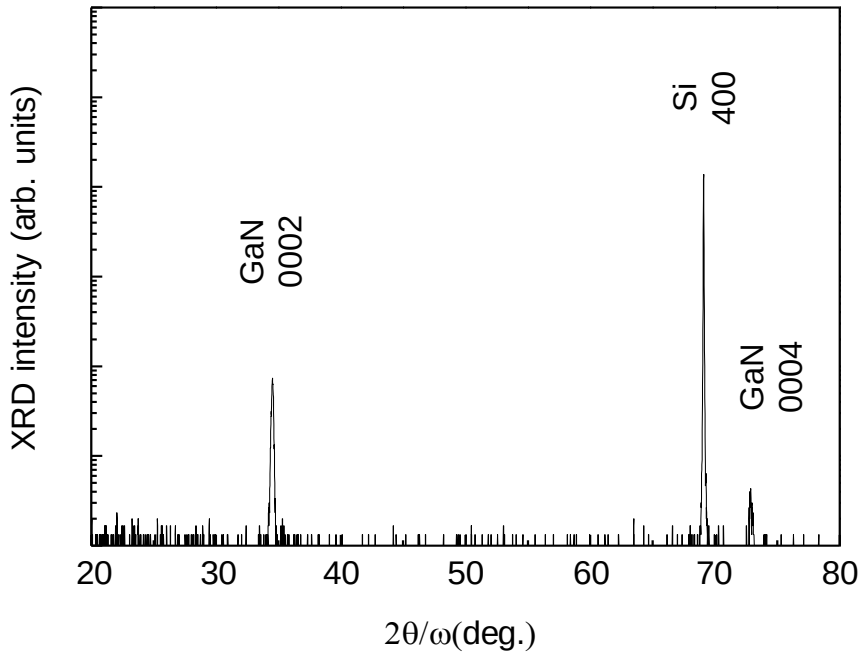

Figure 2-2 XRD pattern of the GaN films grown on the MLG/SiO_2 layers.

2.4 Phase analysis of GaN films

Figure 2-3 shows the EBSD phase map for the GaN films grown at 750°C. The wurtzite and zincblende phases coexist in the GaN films and the ratio of zincblende to wurtzite (zincblende/wurtzite) phases was as high as 0.66. This suggests that the phase purity of the GaN

film is poor. GaN was a mixture of wurtzite and zincblende structure, even though it had been grown on hexagonal MLG. Hence, the structure of the buffer layer is not the only factor for determining the crystal structure of the GaN.

The room-temperature PL (RT-PL) spectrum showed clear excitonic emission from zincblende GaN at approximately 380 nm [2.16, 2.17] together with the near-band-edge emission of wurtzite GaN at approximately 360 nm (Figure 2-4). The broad peak at 550 nm was assigned to defect-related yellow luminescence, which might be due to gallium vacancies or incorporation of carbon into GaN [2.18, 2.19]. The PL spectrum also suggests the coexistence of wurtzite and zincblende phase GaN.

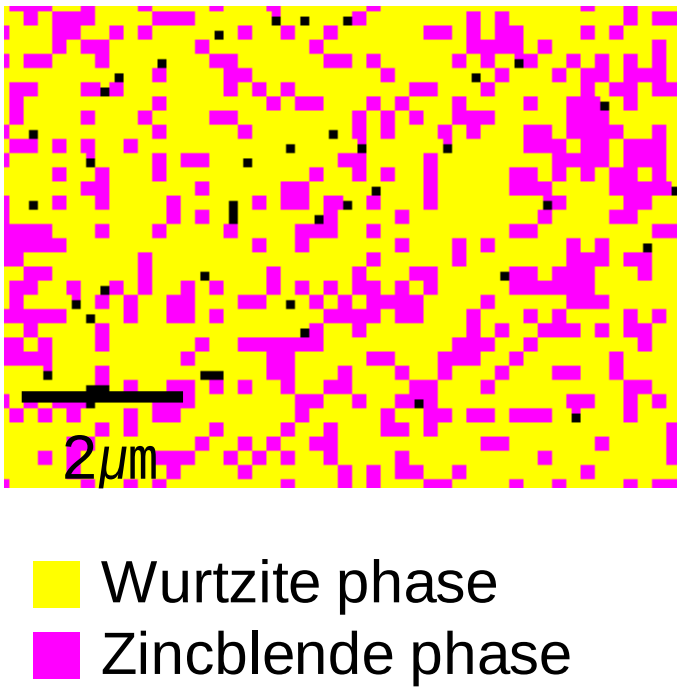

Figure 2-3 EBSD phase map of the GaN film grown on MLG/SiO_2 layers.

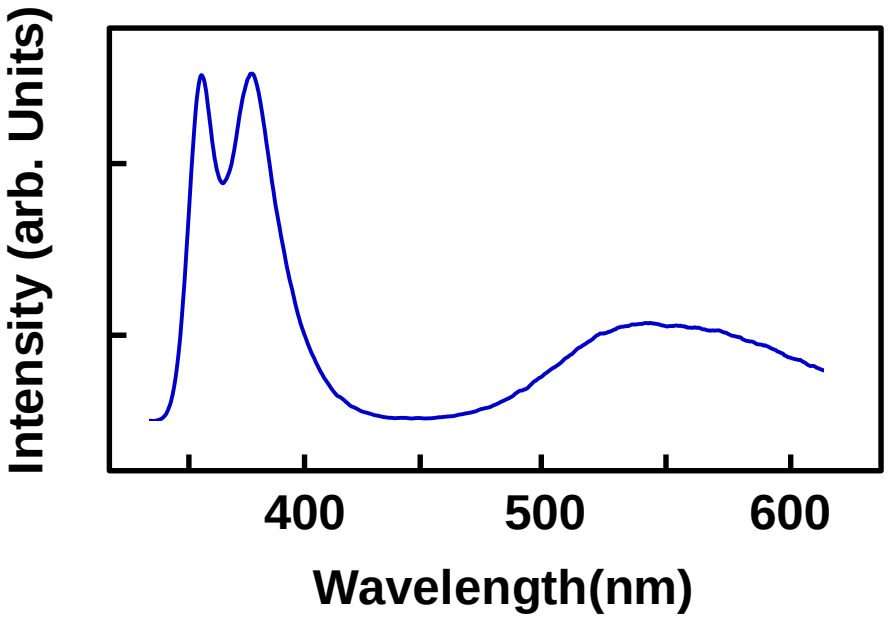

Figure 2-4 RT-PL spectrum of the GaN film grown on MLG/SiO_2 layers.

To determine the origin of the inclusion of zincblende phase, GaN films were grown on MLG/SiO_2 layers by changing the growth temperatures from 650 to 950 °C. As a result, the growth temperature increase led to an increase in the zincblende phase in the GaN films. Figure 2-5 shows the dependence of the zincblende/wurtzite ratio on the growth temperature. Because the wurtzite phase GaN is thermodynamically more stable than the zincblende phase GaN at high growth temperatures, the increase in the zincblende/wurtzite ratio with increasing growth temperature suggests the origin of this the zincblende phase is not due to thermodynamics. An interfacial reaction between GaN and MLG might explain this phenomenon. To check this assumption, 50-nm-thick AlN interlayers were inserted between the GaN and MLG layers to reduce the interfacial reactions. Figure 2-6 shows the sample structure of GaN grown on MLG with AlN interlayer.

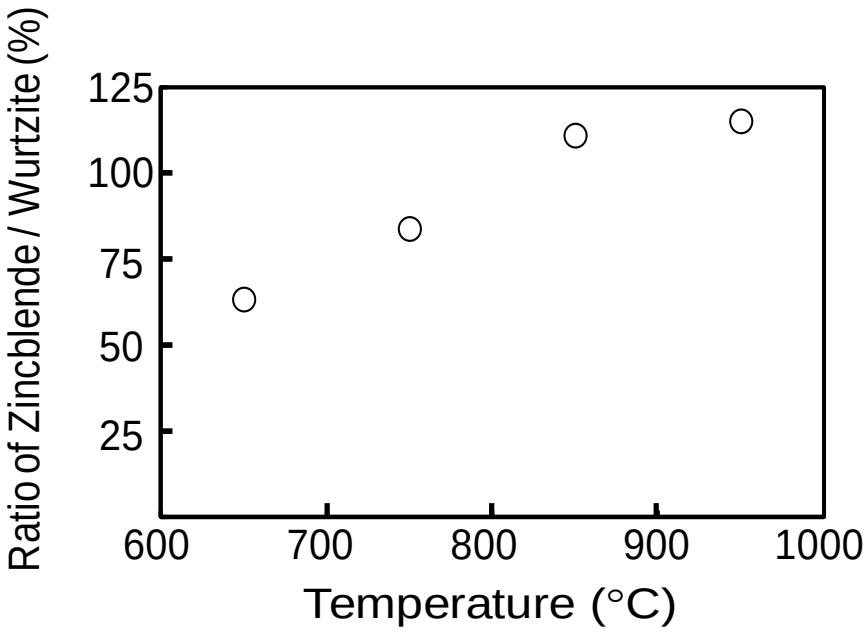

Figure 2-5 Dependence of the zincblende/wurtzite ratio on the growth temperatures.

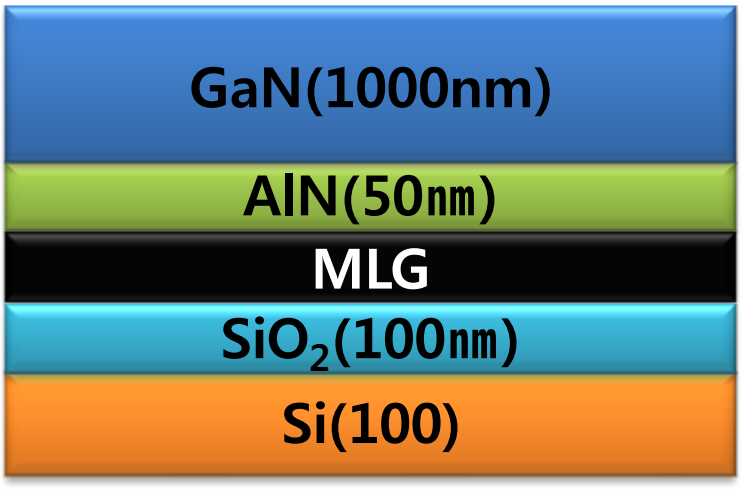

Figure 2-6 A schematic illustration of GaN grown on MLG with AlN interlayer.

Figure 2-7 presents the EBSD phase map for GaN films with AlN interlayers. The concentration of the zincblende phase GaN was almost negligible and the phase purity of wurtzite GaN improved drastically owing to the AlN interlayers. Figure 2-8 shows the dependence of the zincblende/wurtzite ratio on the growth temperature in which GaN films were grown on the AlN/MLG/SiO_2 layers. The amount of zincblende phase GaN remained unchanged, when the growth temperature of GaN was changed from 740 to 810 °C.

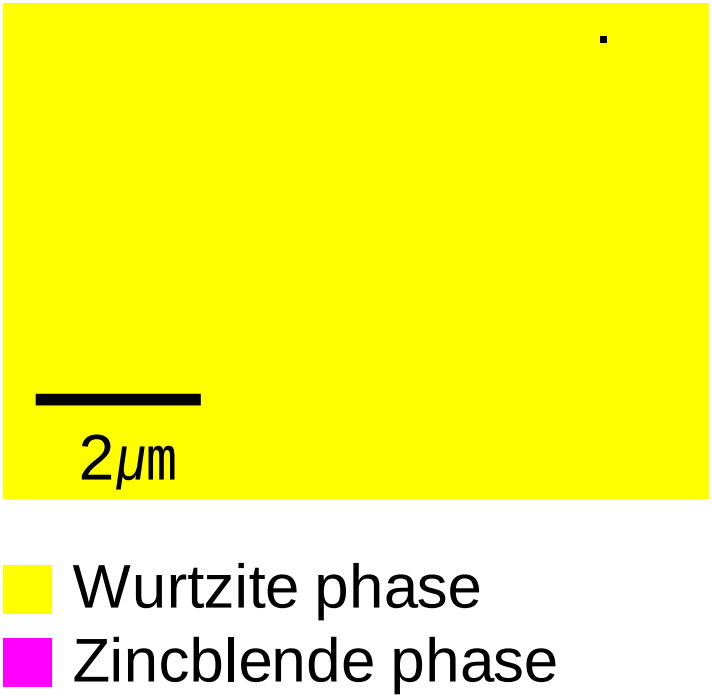

Figure 2-7 EBSD phase map of the GaN film grown on the AlN/MLG/SiO_2 layers.

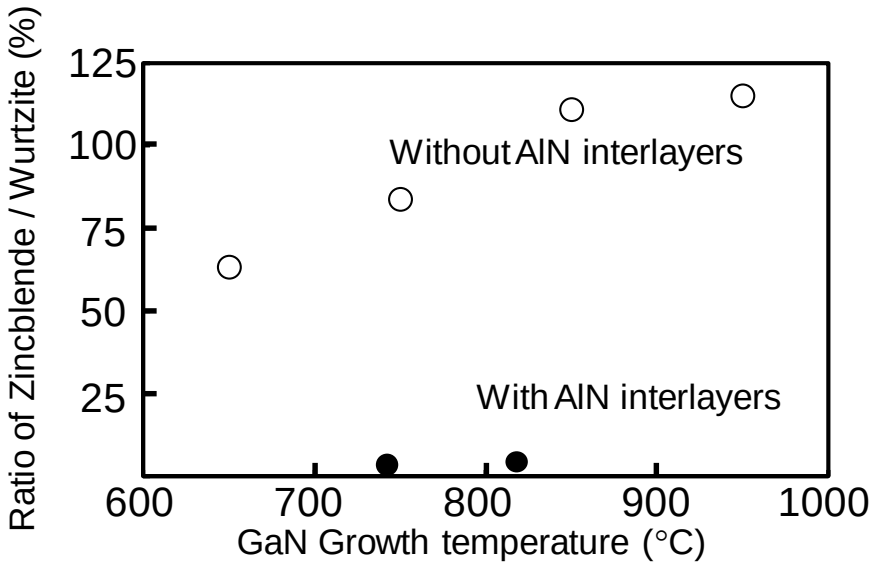

Figure 2-8 Dependence of the zincblende/wurtzite ratio on the growth temperatures.

The RT-PL spectrum of the GaN films with the AlN interlayers showed strong near-band-edge emission from the wurtzite phase and negligible emission from the zincblende phase, as shown in Figure 2-9. This result is consistent with the EBSD results. Furthermore, the decrease in the broad peak at 550 nm suggests improved crystal quality for the GaN films.

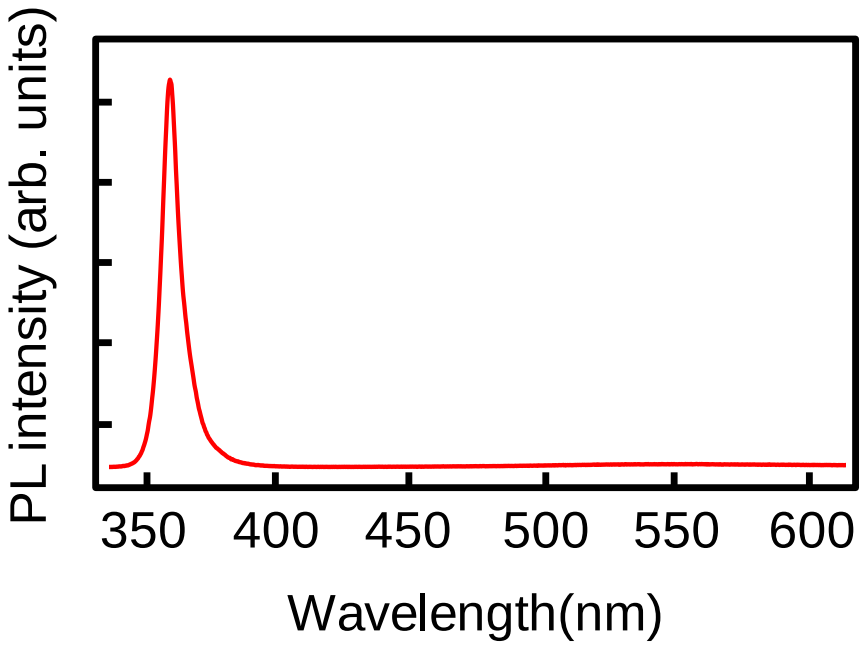

Figure 2-9 A RT-PL spectrum of the GaN film grown on AlN/MLG/SiO_2 layers.

2.5 Crystal quality of GaN films

Figure 2-10 shows the X-ray rocking curves for the 0002 diffractions of the GaN films grown on amorphous SiO_2 without and with AlN interlayers. The full width at half maximum (FWHM) value decreased from 2.40° to 0.62° with the AlN interlayers. This suggests that the insertion of AlN interlayers contributes to the growth of high quality GaN films on MLG.

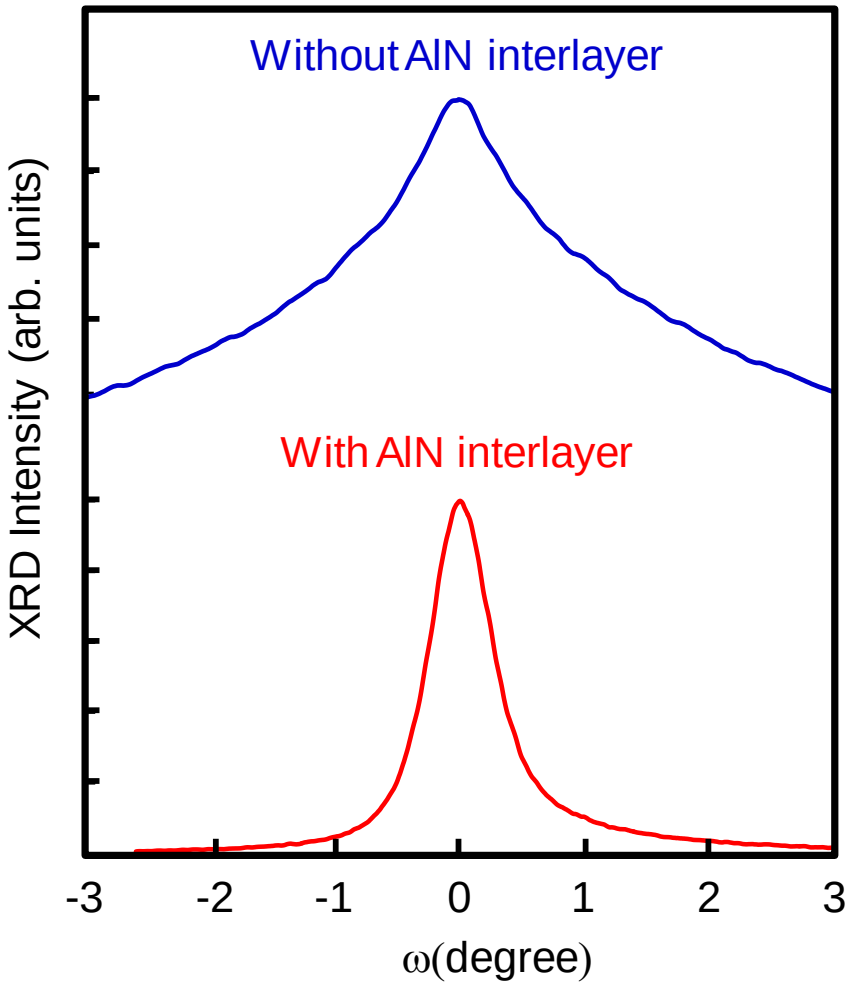

Figure 2-10 X-ray rocking curves of GaN 0002 with and without AlN interlayers.

2.6 Surface morphologies of GaN films

Atomic force microscopy (AFM) of the pristine graphene surfaces revealed a flat surface with Ra = 0.185 nm, as shown in Figure 2-11. On the other hand, the MLG layers grown on Ni with CVD have unavoidable wrinkles and height differences between the flat graphene surfaces and wrinkles. The height differences varied from several nm to several tens nm. Figure 2-12 shows SEM images of the surface morphology of MLG: (a) top view and (b) bird's eye view.

The images show the wrinkles that originate from the difference in coefficients of thermal expansion (CTE) between the MLG and nickel [2.20].

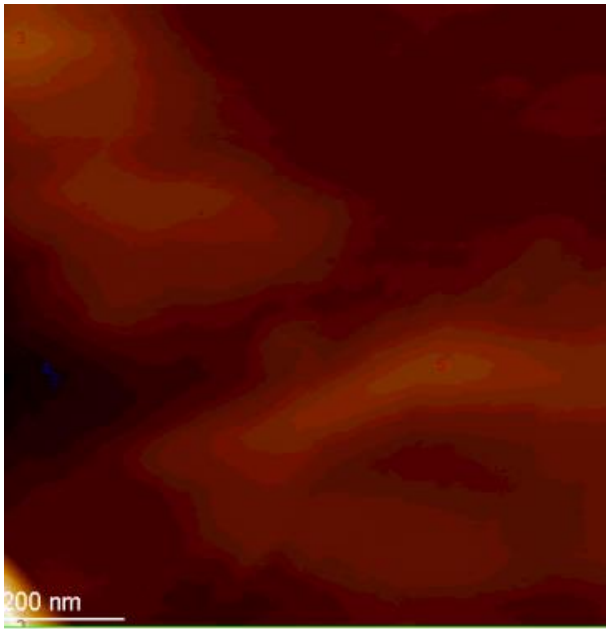

Figure 2-11 AFM image of MLG.

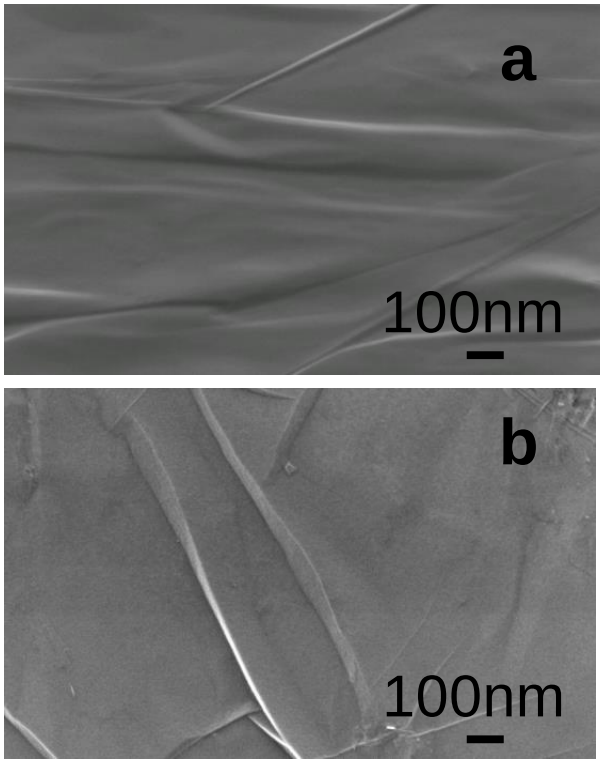

Figure 2-12 SEM images of MLG (a) bird's eye view (b) top view.

In the case of the thin group III- nitride films, the surface morphology of the films is in accordance with the characteristics of MLG. Figure 2-13 presents a SEM image of 50 nm AlN film grown on MLG, showing a similar rough surface morphology. On the other hand, the surface flatness increased with increasing film thickness and flat surface group III-nitrides films were obtained.

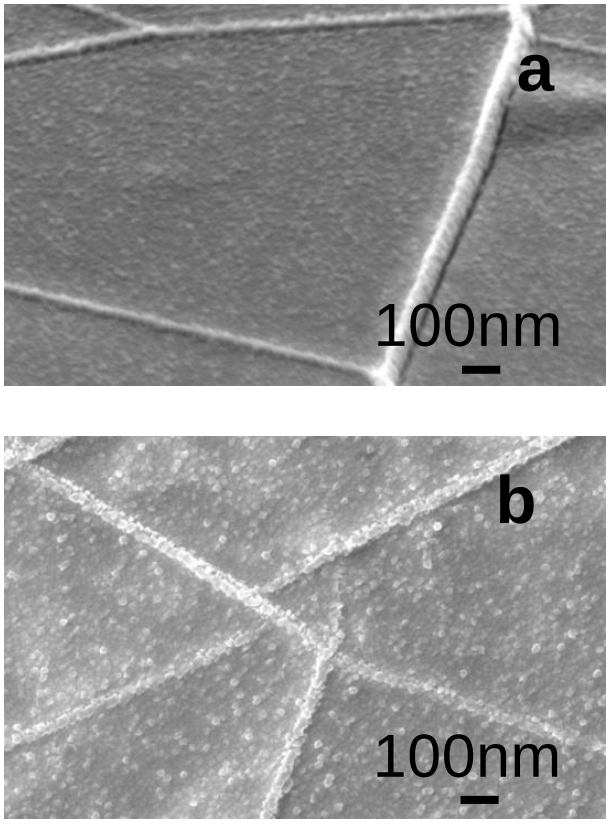

Figure 2-13 SEM images of AlN/MLG (a) bird's eye view (b) top view.

The amorphous nature of the SiO_2 substrates generates random orientations of group III-nitride films with rough surface morphology. The SEM image of GaN films grown on SiO_2 substrate in Figure 2-14 shows a very rough surface morphology. The random orientation and

rough surface of the GaN films indicate that the surface morphology requires further improvement.

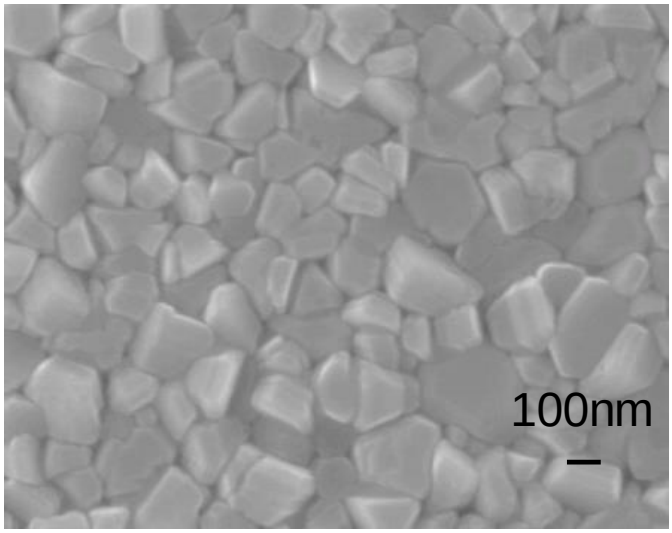

Figure 2-14 SEM image of GaN grown on SiO_2 substrate.

The crystalline structure of MLG imposes regularity on the GaN films and improves the surface morphology. Figure 2-15 shows the dramatic reduction in inclined GaN, which suggests an improvement in crystallinity. On the other hand, the direct growth of GaN on the MLG buffer leads to low phase purity owing to the coexistence of wurtzite and zincblende phases.

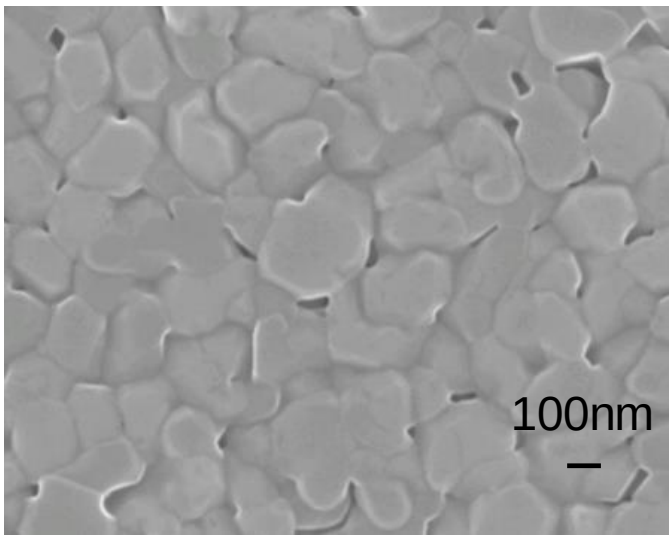

Figure 2-15 SEM image of GaN grown on a SiO_2 substrate with MLG.

As shown in sec. 2.4, the AlN interlayers suppress the formation of the zincblende phase. This method is not only effectively eliminates the zincblende phase GaN but also improve the surface morphology. The smooth surface of GaN grown on AlN/MLG/SiO_2 is shown (Figure 2-15).

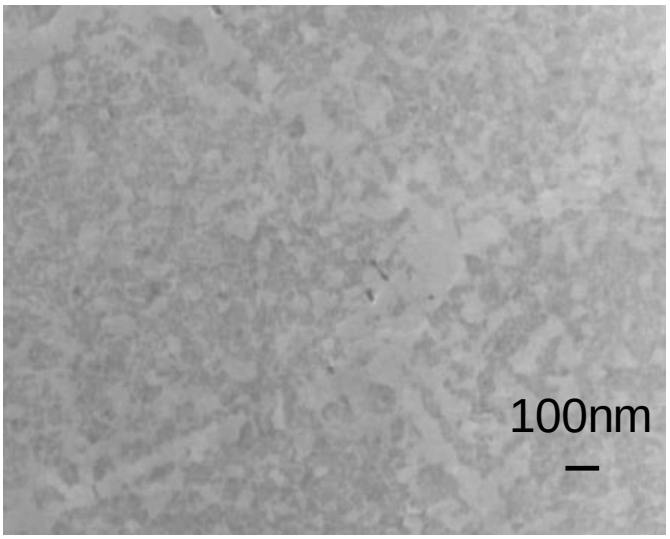

Figure 2-16 SEM image of GaN grown on AlN/MLG/SiO_2.

Figures 2-17 show EBSD pole figures of the GaN films over a 5 × 5 μm^2 area. In Figure 2-17 (a), the {10$\bar{1}$2} pole figure of GaN without an AlN interlayer forms broad ring shaped patterns. This suggests that the crystalline quality of the GaN films is poor with random orientation in the in-plane directions. In contrast, the {10$\bar{1}$2} pole figure of the GaN with AlN interlayer shows a clear six-fold rotational symmetry (Fig. 2-17 (b)). This indicates the absence of zincblende phase and the increase in phase purity. Moreover, the crystalline quality of the GaN films can be improved drastically using the AlN interlayers.

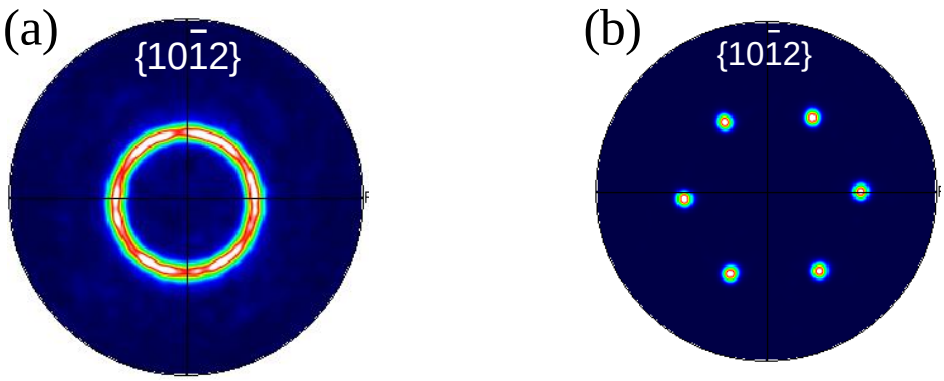

Figure 2-17 EBSD pole figures for GaN films (a) without and (b) with AlN interlayers.

2.7 Polarity of GaN films

The polarity of the GaN films on the MLG buffer layers with AlN interlayers was examined because the polarity control of the GaN films is inherently important to the design of device structures [2.21]. Figure 2-18 (a) shows an SEM image of the GaN surface after KOH etching. The surface showed serious roughening after etching. This chemical vulnerability is a

typical feature of N-polar GaN [2.22]. To develop the controllability of the GaN polarity on MLG, a technique that induces polarity inversion from N- to Ga-polarity is needed. Recently, it was reported that the formation of AlO_x layer on N-polar bulk GaN substrate leads to the subsequent growth of Ga-polar GaN [2.23]. This study introduced the thermal surface oxidization of the AlN interlayers at 200 °C in air to form the AlO_x layers, followed by the growth of GaN films. The surface morphology of the GaN films with the surface-oxidized AlN interlayers remained unchanged after KOH etching as shown in Fig. 2-18 (b), which suggests the formation of Ga-polar GaN films. These results clearly show that the use of AlN interlayers with and without surface oxidization leads to the formation of Ga- and N-polar GaN films on the MLG buffer layers, respectively.

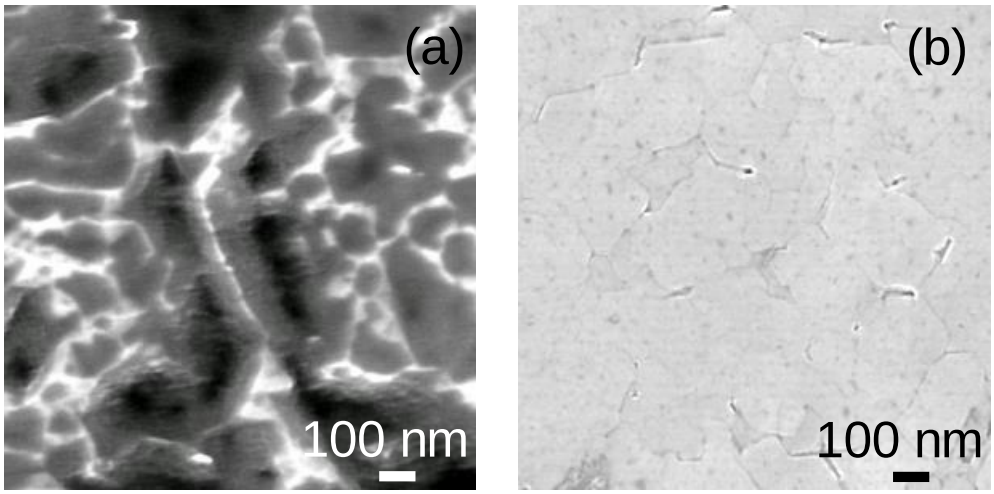

Figure 2-18 SEM images of the GaN films with (a) AlN and (b) surface-oxidized AlN interlayers.

AFM (Figure 2-19) showed that GaN, which was grown on surface-oxidized AlN/MLG/SiO_2, had smooth surface morphology with a roughness of 0.39nm base on the root-means-square (RMS) value.

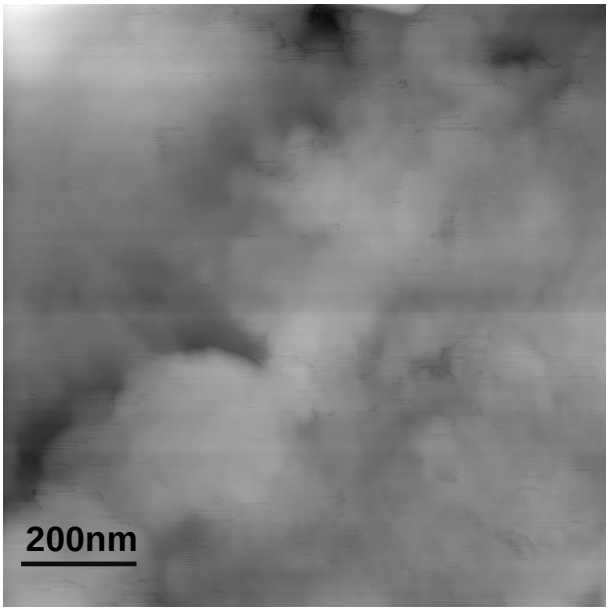

Figure 2-19 2 x 2 μm^2 AFM image of GaN grown on surface-oxidized AlN/MLG/SiO_2.

2.8 Growth temperature reduction of GaN films

The possibility of reducing the growth temperature of GaN films grown on quartz substrates with MLG by PSD was assessed. The MLG buffer layers were grown by CVD and transferred to the quartz surfaces. Before the growth of the group III-nitride films, the MLG/ 2 × 2 cm^2 quartz substrates were degassed at 400 °C for 30 min in vacuum. The growth of GaN and AlN films was performed by a PSD apparatus with a background pressure of 1.0×10^{-10} Torr. The growth temperatures of the GaN and AlN films were set at 500-550 °C. Sputtering of Ga and Al

targets was performed in a N_2/Ar gaseous ambient. The previous section showed that the use of an AlN interlayer and the thermal oxidization of the AlN layer improves the quality of Ga-polar in the sec. 2-7 GaN film. The AlN layers were grown on MLG/ quartz and the AlN surfaces were thermally oxidized.

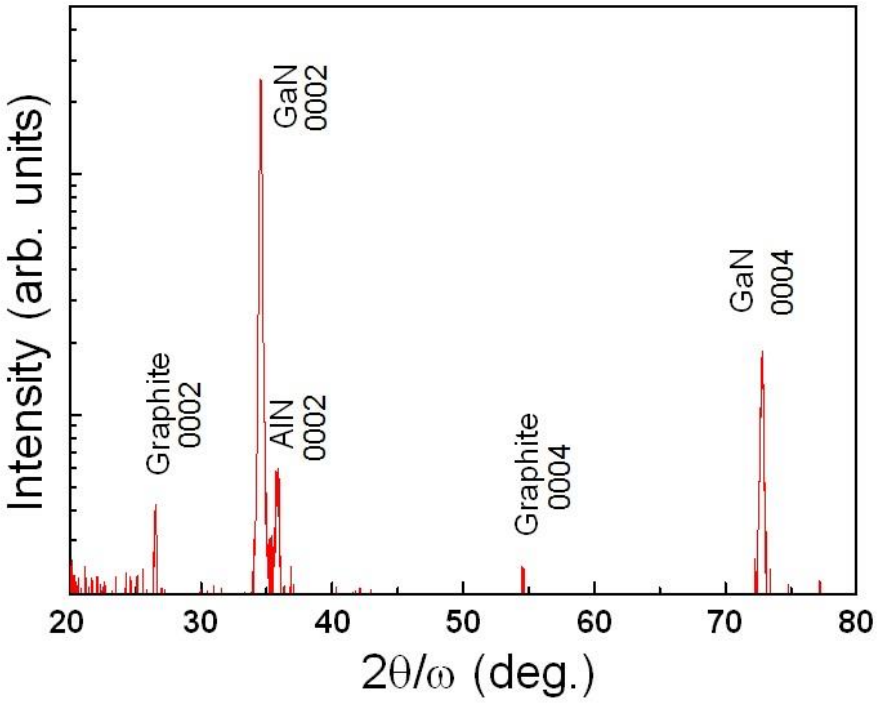

Figure 2-20 XRD curve of the GaN films grown at 550 °C on surface-oxidized AlN/MLG/quartz.

Figure 2-20 shows the XRD 2θ/ω curve of GaN films grown at 550 °C on surface-oxidized AlN/MLG/quartz. Strong XRD peaks were observed at approximately 34.5°, 36.0°, and 72.9°. These peaks correspond to the diffractions from GaN 0002, AlN 0002, and GaN 0004, respectively. This shows that the *c*-axis oriented GaN and AlN films were grown successfully on amorphous quartz, even at low growth temperatures.

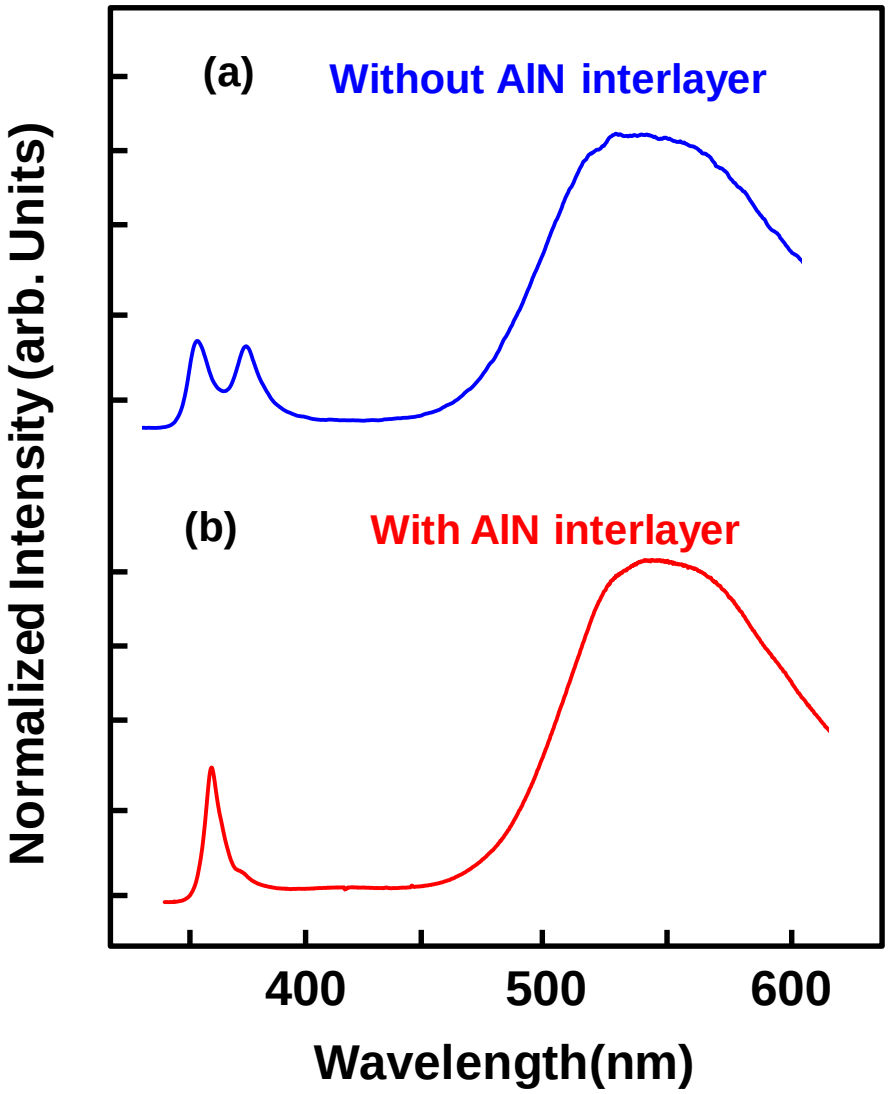

Figure 2-21 RT-PL spectra of the GaN film grown on MLG/quartz at 550 °C (a) without and (b) with an AlN interlayer.

Figure 2-21 shows the room-temperature (RT) PL spectra of the GaN films grown on MLG/quartz at 550 °C. The PL spectrum of the GaN films directly grown on the MLG buffer layer has three peaks as shown in Figure 2-21 (a). Emissions from wurtzite GaN, zincblende GaN, and defect-related yellow luminescence were observed at 360 nm, 380 nm, and 550nm, respectively. On the other hand, strong near-band-edge emissions from the wurtzite phase GaN

and defect-related yellow luminescence were observed in the room-temperature PL spectrum of the GaN films grown on surface-oxidized AlN/MLG/quartz at 550 °C as shown in Figure 2-21 (b). Emissions from zincblende GaN were dramatically reduced probably owing to the suppression of the heterointerface reactions of GaN/MLG using the AlN interlayers. The strong yellow luminescence suggests the high density of point defects, such as Ga vacancies.

2.9 Summary

GaN films were grown on amorphous SiO_2 with MLG buffer layers by PSD, and their structural properties were investigated. The GaN films exhibited *c*-axis oriented structures. The zincblende and wurtzite phases coexisted in the GaN films grown with the MLG buffer layers, whereas the insertion of AlN interlayers resulted in significant improvement in the phase purity of wurtzite GaN in these films. The use of the AlN interlayers with and without surface oxidization led to the formation of Ga- and N-polar GaN films, respectively. In addition, GaN films were successfully grown on quartz with MLG buffer layer even at low temperatures (less than 550 °C), which is applicable to GaN growth on glass. These results clearly show that the use of MLG buffer layers and the introduction of AlN interlayers contribute to the growth of high quality GaN films on amorphous SiO_2, which opens up the possibility of large-area GaN-based devices on SiO_2 substrates.

References

[2.1] S. Nakamura, M. Senoh, S. Nagahama, N. Iwasa, T. Yamada,T. Matsushita, H. Kiyoku, Y. Sugimoto, T. Kozaki, H. Umemoto, M. Sano, and K. Chocho, Jpn. J. Appl. Phys. **36**, L1568 (1997).

[2.2] I. Akasaki, and H. Amano, Jpn. J. Apppl. Phys. **36**, 5393 (1997).

[2.3] H. Amano, N. Sawaki, I Akasaki, and Y. Toyoda, Appl. Phys. Lett. **48**, 353 (1986)

[2.4] H. Amano, M. Kito, K. Hiramatsu, and I. Akasaki Jpn. J. Appl. Phys. **28**, L2112 (1989).

[2.5] K. Chung, C. H. Lee, and G. C. Yi, Science 330, 655 (2010).

[2.6] D. P. Bour, N. M. Nickel, C. G. Van de Walle, M. S. Kneissl, B. S. Krusor, P. Mei, and N. M. Johnson, Appl. Phys. Lett. 76, 2182 (2000).

[2.7] S. Guha and N. A. Bojarczuk, Appl. Phys. Lett. 72, 415 (1998).

[2.8] A. Kobayashi, H. Fujioka, J. Ohta, and M. Oshima, Jpn. J. Appl. Phys. 43, L53 (2004).

[2.9] J. Ohta, H. Fujioka, and M. Oshima, Appl. Phys. Lett. 83, 3060 (2003).

[2.10] S. Inoue, K. Okamoto, T. Nakano, J. Ohta, and H. Fujioka, Appl. Phys. Lett. 91, 201920 (2007).

[2.11] S. Garner, et al., Flexible Electronics and Displays Conference, February **9**, Corning, (2011)

[2.12] K. Sato, J. Ohta, S. Inoue, A. Kobayashi, and H. Fujioka, Appl. Phys. Express 2, 011003 (2009).

[2.13] K. Okubo, A. Kobayashi, J. Ohta, M. Oshima, and H. Fujioka, Appl. Phys. Lett. 102, 022103 (2013).

[2.14] X. S. Li, W. W. Cai, J.H. An, S. Kim, J. Nah, D. X. Yang, R. D. Piner, A. Velamakanni, I.

Jung, E. Tutuc, S. K. Banerjee, L. Colombo, and R. S. Ruoff, Science **324**, 1312 (2009).

[2.15] C. Trager-Cowan, F. Sweeney, A. J. Wilkinson, and I. M. Watson, P. G. Middleton, K. P. O'Donnell, D. Zubia, S. D. Hersee, S. Einfeldt, and D. Hommel, Phys. stat. Sol. (c) **0**, 532 (2002).

[2.16] S. Strite, J. Ruan, Z. Li, A. Salvador, H. Chen, D. J. Smith, W. J. Choyke, and H. Morkoc, J. Vac. Sci. Technol. B 9, 1924 (1991).

[2.17] J. Menniger, U. Jahn, O. Brandt, H. Yang, and K. Ploog, Phys. Rev. B 53, 1881 (1996).

[2.18] R.Y. Korotkov, M.A. Reshchikov, and B.W. Wessels, Physica B 325 (2003).

[2.19] J.I. Lyons, A. and Janotti, C.G. Van, Appl. Phys. Lett. 59,1749 (2010).

[2.20] K. S. Kim, Y. Zhao, H. Jang, S. Y. Lee, J. M. Kim, K. S. Kim, J. H. Ahn, P. Kim, J.Y. Choi, and B. H. Hong, Nature. 457, 706 (2009)

[2.21] Hadis Morkoc, Aldo Di Carlo, and Roberto Cingolani, Solid-State Electron. 46, 157 (2002)

[2.22] J.L. Weyher, S. Miiller, I. Grzegory, and S. Porowski, J. Cryst. Growth **182**, 17 (1997).

[2.23] M. H. Wong, F. Wu, J. S. Speck, and U. K. Mishra, J. Appl. Phys. **108**, 123710 (2010).

Chapter 3

Strain analysis of the GaN films

3.1 Introduction

Group III-nitride substrates are mainly grown heteroepitaxially, because of the limited availability of GaN bulk substrates. The use of foreign substrates normally causes large mismatch in lattice constants and thermal expansion coefficients between GaN and the substrates. These mismatches generate strain in the films, which significant affects the structural, electrical, and optical properties of the films. In this chapter, a technique for assessing the generation of strain, as well as the growth of group III-nitrides on MLG is reported.

3.2 Origin of strain and stress

The strain in the films is defined as the change in lattice parameters relative to the bulk lattice constants. Strain is a second rank tensor quantity denoted with the symbol ε_{kl}. Stress is the force per unit area acting on the material to cause deformation. Stress is also a second rank tensor quantity denoted with the symbol σ_{ij}. The most general tensor in the form of Hooke's law relates the stress to the strain through the fourth order stiffness tensor, c_{ijkl}, as shown in Equation 3-1:

$$\sigma_{ij} = c_{ijkl}\varepsilon_{kl} \qquad i,j,k,l = 1,2,3. \qquad \text{(Equation 3-1)}$$

Each of the nine equations in Equation 3-1 requires nine constants to describe the state. Therefore, 81 constants are needed to calculate the stiffness tensor. Because the stress and strain tensors have a symmetrical nature, (i.e. $\varepsilon_{kl} = \varepsilon_{lk}$, $\sigma_{ij} = \sigma_{ji}$), the number of independent constant can be reduced. Figure 3-1 shows the symmetric nature of the tensors. The number of independent constants may be reduced by the symmetry and geometry of the material system.

Figure 3-1 Symmetric nature of tensors.

In the case of films with hexagonal symmetry, the biaxial modulus (M) of the (0001) plane can be given by Equation 3-2:

$$M_{0001} = \left[(C_{11} + C_{12}) - \frac{2(C_{13})^2}{C_{33}}\right], \qquad \text{(Equation 3-2)}$$

where c_{ij} (i,j=1,2,3) are the elastic constants of group III-nitrides.

The shear modulus is presented as C_{44} in the (0001) plane. The Poisson ratio (ν), the fraction of compression divided by the fraction of expansion that expands perpendicularly to the direction of compression, is expressed with Equation 3-3:

$$\nu = \frac{C_{13}}{C_{13}+C_{33}} \ . \qquad \text{(Equation 3-3)}$$

Stress, which is the origin of strain, can be classified roughly into the following two groups: intrinsic stress and extrinsic stress. Extrinsic stresses are imposed on the films from the outside environment, e.g. difference in the CTE between the substrates and films. The intrinsic stresses originate from the films themselves during growth on substrates. Heteroepitaxy, grain coalescence, and grain growth can produce intrinsic stress. Hereafter, a brief discussion of such stresses is provided to help develop a fundamental understanding of the strain evolution.

Thermal stress arises when the film and substrate have differences in the CTE and undergo a temperature change. The strain generated by this thermal stress is described by Equation 3-4[3.1]:

$$\varepsilon = -\int_{T_i}^{T}(\alpha_f(T) - \alpha_s(T))dT \approx -(\alpha_f(T) - \alpha_s(T))\Delta T, \qquad \text{(Equation 3-4)}$$

where ε is the strain, α_f and α_s are the linear CTE of the film and substrate respectively, T is the final temperature and T_i is the initial temperature.

When the films are grown on different substrate materials, the heteroepitaxial strain can be expressed as Equation 3-5[3.2]:

$$\varepsilon \approx \frac{a_s - a_f}{a_f}, \qquad \text{(Equation 3-5)}$$

where a_f and a_s are the lattice constant of the film and substrate, respectively.

Tensile stress is induced at the initial stages of grain coalescence to form a continuous film. This mechanism was first proposed by Hoffman [3.3] and improved by Nix and Clemens in

metallic films [3.2]. Sheldon proposed an improved model that explains the tensile stress portion of the stress generation during the deposition of AlN by MBE [3.4].

Tensile stress generation by grain growth in polycrystalline metal films was first proposed by Chaudhari [3.5] and improved by Doerner and Nix [3.6] and Koch [3.7]. Grain boundaries have lower atomic density, which is associated with excess volume, than the bulk. This excess volume reduction generates tensile stresses. The strain energy that accompanies with this stress increases as the grains grow. Therefore, to remain thermodynamically favourable, this type of strain energy must be compensated for by a decrease in the grain boundary energy.

3.3 Techniques for measurements of strain and stress in group III-nitride film

Strain and stress in group III-nitride films can be measured using several techniques. . *Ex-situ* XRD is used most frequently to measure strain. On the other hand, *In- situ* measurements are particularly important because the strain in group III-nitrides is easily affected by post-growth processes (i.e. cooling and heating). *In- situ* studies have been performed for the MOCVD grown group III-nitride on sapphire [3.8] and silicon [3.9]. On the other hand, there are no reports of *In- situ* strain studies during the PSD growth of group III-nitrides. Therefore, it is valuable to apply *In- situ* techniques to understand the growth of group III-nitride on graphene by PSD. *In- situ* optical curvature measurements system were developed in this study to determine the relative changes in the strain during PSD growth.

3.3.1 *Ex- situ* XRD measurements

Hexagonal wurtzite GaN grown on sapphire substrates is the most commonly used material among group III-nitride materials. The crystallographic structure of the wurtzite GaN column belongs to the hexagonal space group. Therefore, the a and b crystallographic axes of the wurtzite GaN were oriented practically parallel to the (0001) plane of the sapphire substrate. For this reason, the GaN epilayer shows in-plane isotropic elastic properties, and its in-plane deformation state can be described by a single strain component. Figure 3-2 shows stressed unit cell of GaN.

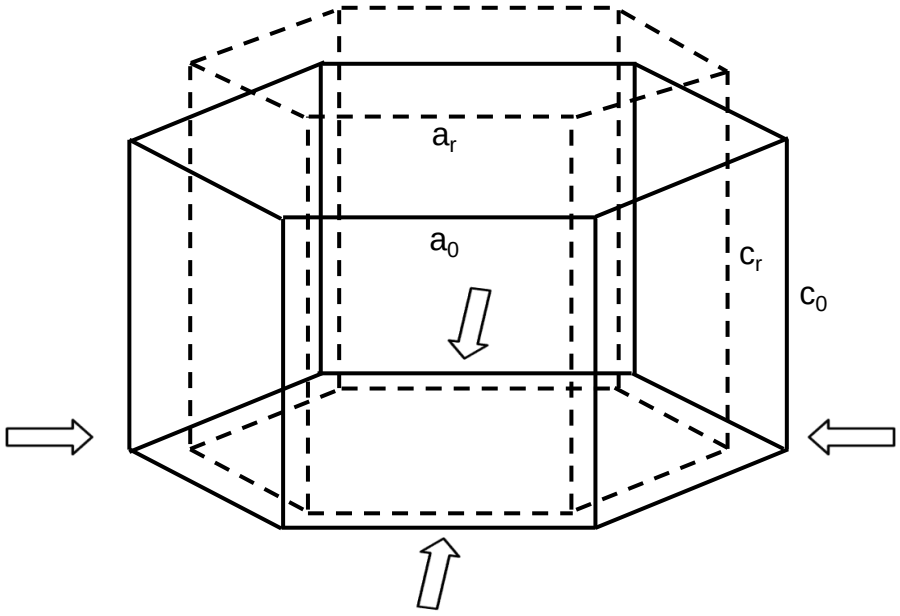

Figure 3-2 Schematic diagram of the stressed unit cell of GaN.

The out-of-plane strain of the GaN film can be described by ε_c as shown by Equation 3-6:

$$\varepsilon_{zz} = \varepsilon_c = \frac{c_r - c_0}{c_0} \ , \qquad \text{(Equation 3-6)}$$

where c_0 and c_r are the unstrained and real c-lattice constants respectively.

The in-plane strain of the GaN film can be described by ε_a, as shown by Equation 3-7:

$$\varepsilon_{xx} = \varepsilon_{yy} = \varepsilon_a = \frac{a_r - a_0}{a_0} \ , \qquad \text{(Equation 3-7)}$$

where a_0 and a_r are the unstrained and real a-lattice constants respectively [3.10].

Using the Poisson ratio ν, Equations 3-8, and 3-9 represent the relation between each strain component:

$$\varepsilon_c = -2\frac{c_{13}}{c_{33}}\varepsilon_a \ , \qquad \text{(Equation 3-8)}$$

$$\varepsilon_c = -\frac{2\nu}{1-\nu}\varepsilon_a \ . \qquad \text{(Equation 3-9)}$$

The c-lattice constant of the GaN films was measured from the θ/2θ diffraction spectra using the Bragg symmetrical set-up, as shown Figure 3-3.

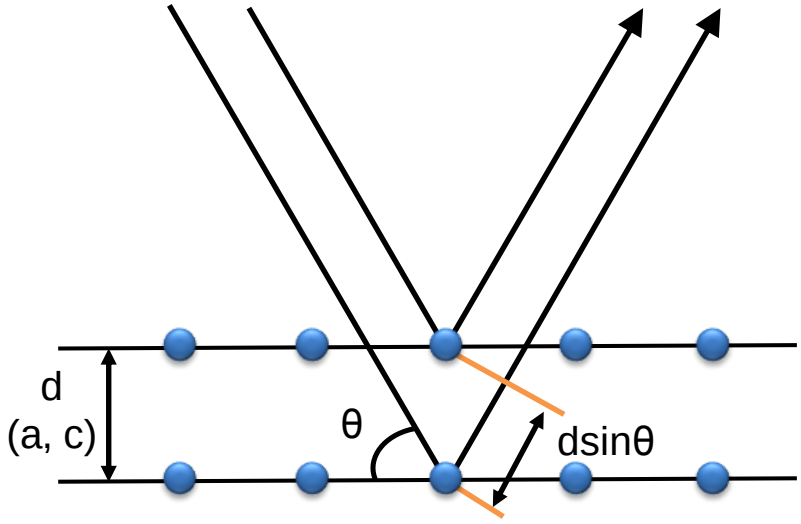

Figure 3-3 Schematic diagram of the XRD measurement.

The curves of GaN, 0002, 0004, and 0006, were recorded from θ/2θ scans and used to evaluate the real c-lattice constant. The real value of the c-lattice constant, c_r, and its experimental value, c_h, are connected through the angular parameter, p_h, as shown in Equations 3-10, 3-11,and 3-12:

$$c_h = -D\frac{c_r}{r}p_h + c_r \ , \qquad \text{(Equation 3-10)}$$

$$p_h = \frac{Cos^2\theta_h}{Sin\theta_h} \ , \qquad \text{(Equation 3-11)}$$

$$c_h = \frac{h\lambda}{2Sin\theta_h} \ . \qquad \text{(Equation 3-12)}$$

θ_h is the angular position of the GaN 000h (h = 2, 4, 6; h is the order of reflection) XRD peak in θ-scale, c_h is the value of the c-lattice parameter determined from the angular position of the 000h diffraction peak, r is the distance of the specimen detector, D is a possible displacement of the specimen with respect to the goniometer axis in the equatorial plane, and λ is the wavelength of x-ray. The lattice parameter, c_r, was determined from the plots {p_h, c_h} using the standard extrapolating technique.

The out-of-plane strain, ε_c, was determined from Equation 3-10 for the average c_r value and the unstrained lattice parameter, c_0 = 0.5185 nm, measured for the homoepitaxially grown GaN films [3.11]. In a similar manner, using the plot {p_{hkil}, a_{hkil}}, the in-plane strain was evaluated from the diffraction peaks of the asymmetrical reflections hkil = $10\bar{1}4$, $10\bar{1}5$ and $20\bar{2}4$. The real values of the a-lattice constant, a_r, and its experimental values, a_h, were connected through the angular parameter, p_{hkil}, by the relationship represented in Equations 3-13, 3-14, and 3-15:

$$a_{hkil} = -D\frac{a_r}{r}p_{hkil} + a_r \ , \qquad \text{(Equation 3-13)}$$

$$p_{hkil} = \frac{Cos^2\theta_{hkil}}{Sin\theta_{hkil}} \ , \qquad \text{(Equation 3-14)}$$

$$a_{hkil} = c_r d_{hkil}\sqrt{\frac{\frac{4}{3}(h^2+k^2+hk)}{c_r^2 - l^2 d_{hkil}^2}} \ . \qquad \text{(Equation 3-15)}$$

External biaxial strain and internal hydrostatic strain coexist in the GaN films [3.10]. The biaxial strain originates from lattice mismatch and the difference in CTEs between the GaN films and substrate. The hydrostatic strain originates from the existence of point defects, and the amount of hydrostatic strain is affected by the size of the point defects. Equations 3-16, 3-17 and 3-18 express the relationship between the biaxial strain and hydrostatic strain:

$$\varepsilon_c = \varepsilon_c^b + \varepsilon_h \ , \qquad \text{(Equation 3-16)}$$

$$\varepsilon_a = \varepsilon_a^b + \varepsilon_h \ , \qquad \text{(Equation 3-17)}$$

$$\varepsilon_h = \frac{1-\nu}{1+\nu}\left(\varepsilon_c + \frac{2\nu}{1+\nu}\varepsilon_a\right) \ . \qquad \text{(Equation 3-18)}$$

The measured values of ε_c and ε_a are a combination of the biaxial strain, ε^b_c and ε^b_a in the c- and a-directions respectively, and of the hydrostatic strain ε_h. The hydrostatic strain, ε_h, can be determined from ε_c, ε_a, and the Poisson ratio. ν is the Poisson ratio (Equation 3-3) and c_{13} and c_{33} are the elastic constants of GaN. The elastic constants values of GaN c_{13} = 106 GPa and c_{33} = 398 GPa were referenced [3.12].

The in-plane stresses of the c-axis oriented GaN films have biaxial characteristics and can be determined by using Equation 3-19:

$$\sigma_f = M_f \varepsilon_a^b \ , \qquad \text{(Equation 3-19)}$$

where σ_f is the biaxial stress in the films, and M_f is the biaxial elastic modulus for hexagonal GaN films. M_f is described in Equation 3-2, and c_{11} = 390 GPa, c_{12} = 145 GPa, c_{13} = 106 GPa, c_{33} = 398 GPa, respectively [3.12].

3.3.2 Stoney's formula

Equation 3-20 is Stoney's formula, which was first published in 1909 [3.13]:

$$\kappa(t) = \frac{6\sigma(t)h_s(t)}{M_s h_f^2} \ . \qquad \text{(Equation 3-20)}$$

The substrate curvature is related to the film stress $\sigma(t)$ with Stoney's formula, where h_f is the film thickness h_s is the substrate thickness and M_s is the substrate biaxial modulus. As expressed in equation 3-20, the curvature is proportional to the product of the film stress and film thickness, i.e. "stress thickness".

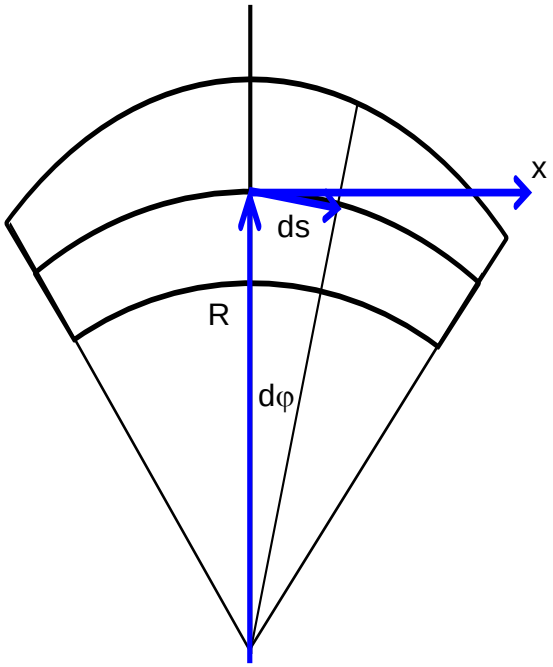

Figure 3-4 Schematic diagram of the curvature of film.

The approximation of Equation 3-21 is valid for small deformation:

$$\kappa(t) = \frac{1}{R} = \frac{d\varphi}{ds} = \frac{(\arctan(w'))'dx}{\sqrt{dx^2+dw^2}} = \frac{w''dx}{(1+w')^{3/2}dx} \cong w'' \quad . \qquad \text{(Equation 3-21)}$$

Figure 3-4 shows a diagram of the curvature of a film, where R is the radius of the curvature, s is the arc length, φ is the angle of the arc and w is the displacement in the z-direction. The approximation of Equation 3-21 is valid for small deformations.

Equation 3-22 shows the basic relation between the deformation u_{ij} and stress components σ_{ij} in a linear elastic material:

$$\sigma_{jk} = \frac{E}{1+\nu}\left(u_{jk} + \frac{\nu}{1-2\nu}u_{ll}\delta_{jk}\right) \quad . \qquad \text{(Equation 3-22)}$$

The film thickness, z, is assumed to be very small compared to the other two directions, x and y, and stress components of these direction are negligible amount. As shown Equation 3-23, all shear stresses vanish:

$$\sigma_{xz} = \sigma_{yz} = 0. \qquad \text{(Equation 3-23)}$$

From Equation 3-21, the normal deformation of each direction can be estimated with $z=\alpha$ being the position of a neutral surface, which is the position free of force and torque. Equations 3-24, 3-25 and 3-26 show the relation between the deformation of each direction and displacement in the z-direction:

$$u_{xx} = -(z-\alpha)\frac{\partial^2 w}{\partial x^2} \ , \qquad \text{(Equation 3-24)}$$

$$u_{yy} = -(z-\alpha)\frac{\partial^2 w}{\partial y^2} \ , \qquad \text{(Equation 3-25)}$$

$$u_{zz} = \frac{(z-\alpha)\nu}{1-\nu}\left(\frac{\partial^2 w}{\partial x^2} + \frac{\partial^2 w}{\partial y^2}\right) \ . \qquad \text{(Equation 3-26)}$$

The normal stress of each direction, Equations 3-27 and Equations 3-28, can be obtained by combining Equations 3-22 and 3-23:

$$\sigma_{xx} = \frac{E}{(1+\nu)(1-2\nu)}\left[(1-2\nu)u_{xx} + \nu(u_{yy}+u_{zz})\right] \ , \qquad \text{(Equation 3-27)}$$

$$\sigma_{yy} = \frac{E}{(1+\nu)(1-2\nu)}\left[(1-2\nu)u_{yy} + \nu(u_{xx}+u_{zz})\right] \ . \qquad \text{(Equation 3-28)}$$

Putting equations 3-24, 3-25 and 3-26 into Equations 3-27 and 3-28 and simplifying gives Equations 3-29 and Equations 3-30:

$$\sigma_{xx} = \frac{Ez}{(1-\nu^2)}\left[\frac{\partial^2 w}{\partial x^2} + \nu\frac{\partial^2 w}{\partial y^2}\right] , \quad \text{(Equation 3-29)}$$

$$\sigma_{yy} = \frac{Ez}{(1-\nu^2)}\left[\frac{\partial^2 w}{\partial y^2} + \nu\frac{\partial^2 w}{\partial x^2}\right] . \quad \text{(Equation 3-30)}$$

Using Equations 3-29 and 3-30 and the neutral surface condition, the relationship between the normal stress and the thickness can be obtained.

Force:

$$F_x = 0 = \int_0^{h_{tot}} \sigma_{xx}(z)dz = \int_0^{h_s} \frac{E_s}{(1-\nu_s^2)}\left[\frac{\partial^2 w}{\partial x^2} + \nu_s\frac{\partial^2 w}{\partial y^2}\right](z-\alpha)dz + \int_{h_s}^{h_{tot}} \sigma_{xx}^f dz ,$$

(Equation 3-31)

$$F_y = 0 = \int_0^{h_{tot}} \sigma_{yy}(z)dz = \int_0^{h_s} \frac{E_s}{(1-\nu_s^2)}\left[\frac{\partial^2 w}{\partial y^2} + \nu_s\frac{\partial^2 w}{\partial x^2}\right](z-\alpha)dz + \int_{h_s}^{h_{tot}} \sigma_{yy}^f dz ,$$

(Equation 3-32)

Torque:

$$M_x = 0 = \int_0^{h_{tot}} \sigma_{xx}(z)(z-\alpha)dz ,$$

$$M_x = \int_0^{h_s} \frac{E_s}{(1-\nu_s^2)}\left[\frac{\partial^2 w}{\partial x^2} + \nu_s\frac{\partial^2 w}{\partial y^2}\right](z-\alpha)^2 dz + \int_{h_s}^{h_{tot}} \sigma_{xx}^f (z-\alpha)dz ,$$

(Equation 3-33)

$$M_y = 0 = \int_0^{h_{tot}} \sigma_{yy}(z)(z-\alpha)dz ,$$

$$M_y = \int_0^{h_s} \frac{E_s}{(1-\nu_s^2)}\left[\frac{\partial^2 w}{\partial y^2} + \nu_s \frac{\partial^2 w}{\partial x^2}\right](z-\alpha)^2 dz + \int_{h_s}^{h_{tot}} \sigma_{yy}^f (z-\alpha) dz \ .$$

(Equation 3-34)

The position of the neutral surface is determined using Equation 3-31, 3-32, 3-33, and 3-34 as shown in Equation 3-35:

$$\alpha = \frac{h_s(3h_f+2h_s)}{6(h_f+h_s)} \ . \qquad \text{(Equation 3-35)}$$

Using Equation 3-35, the relationship between the normal stresses and film curvature can be obtained as defined in Equation 3-36 and Equation 3-37:

$$\sigma_{xx}^f = -\frac{E_s h_s^3}{6(1-\nu_s^2)h_f(h_f+h_s)}\left[\frac{\partial^2 w}{\partial x^2} + \nu_s \frac{\partial^2 w}{\partial y^2}\right] \cong -\frac{E_s h_s^3}{6(1-\nu_s^2)h_f(h_f+h_s)}\left[\frac{1}{R_x} + \nu_s \frac{1}{R_y}\right] \text{ , (Equation 3-36)}$$

$$\sigma_{yy}^f = -\frac{E_s h_s^3}{6(1-\nu_s^2)h_f(h_f+h_s)}\left[\frac{\partial^2 w}{\partial y^2} + \nu_s \frac{\partial^2 w}{\partial x^2}\right] \cong -\frac{E_s h_s^3}{6(1-\nu_s^2)h_f(h_f+h_s)}\left[\frac{1}{R_y} + \nu_s \frac{1}{R_x}\right] \text{ . (Equation 3-37)}$$

Assuming homogeneous growth of a film, the in-plane stresses of films have an isotropic nature. Equation 3-38 represents isotropic stress and Equation 3-39 isotropic deformation along :

$$\sigma_{xx}^f = \sigma_{yy}^f = \sigma_{rr}^f \ , \qquad \text{(Equation 3-38)}$$

$$\frac{\partial^2 w}{\partial x^2} = \frac{\partial^2 w}{\partial y^2} \quad \rightarrow \quad \frac{1}{R_y} = \frac{1}{R_x} \ . \qquad \text{(Equation 3-39)}$$

Equation 3-40 shows stress along the one-direction:

$$\sigma_{rr}^{f} \cong -\frac{E_s h_s^3}{6(1-\nu_s^2)h_f(h_f+h_s)}\left[\frac{1}{R_r}+\nu_s\frac{1}{R_r}\right] = -\frac{E_s h_s^3}{6(1-\nu_s)h_f(h_f+h_s)}\frac{1}{R_r} \quad . \qquad \text{(Equation 3-40)}$$

If $h_s >> h_f$, Equation 3-40 can be altered to Equation 3-41

$$\sigma_{rr}^{f} \cong= -\frac{E_s h_s^3}{6(1-\nu_s)h_f h_s}\frac{1}{R_r} = -\frac{E_s h_s^2}{6(1-\nu_s)h_f}\frac{1}{R_r} = -\frac{E_s h_s^2}{6(1-\nu_s)h_f}\kappa \quad . \qquad \text{(Equation 3-41)}$$

Equation 3-41 is defined as Stoney's formula.

3.3.3 *In- situ* curvature measurements

Several groups have conducted *In- situ* studies by optical curvature measurements of group III-nitride films on sapphire and Si substrates grown by MOCVD [3.1, 3.2, 3.14~19] but there are no reports on *in- situ* strain for PSD growth of group III-nitrides. Therefore, *in- situ* curvature measurement system was set up for PSD and the strain generation in group III-nitride films was examined.

The curvature measurement system is based on measurements of the deflection of an array of multiple parallel lasers. The system uses a laser light through a highly reflective etalon, which produces multiple arranged beams. The multiple laser beams were incident to the sample at an angle θ from the normal and the reflected beams were directly detected by a CCD camera. Commercial software was used to define and capture the pixel region around each beam and then determine the position and intensity of each beam in real-time.

Curvature measurements provide us information about the stress generated in the samples. The substrate curvature (κ(t)) was determined using Equation 3-42, where L is the distance between the substrate and the detector and $D_{(t)}/D_0$ is the time dependent spacing between the spots normalized by the initial spacing of the measurement system.

$$\kappa(t) = -\frac{\cos\theta}{2L}\left(\frac{D_0 - D(t)}{D_0}\right) = -\frac{\cos\theta}{2L}\left(\frac{\delta D}{D_0}\right) \ . \qquad \text{(Equation 3-42)}$$

If the deposited film is in compressive strain state, the transfer of strain from the film to the substrate will result in the bending of the substrate and films. Consequently, the substrate and film deformation will have convex shape. On the other hand, if the deposited film is in tensile strain state, the substrates and film deform to concave shape.

3.3.4 *In- situ* anisotropic curvature measurements in PSD

Before measuring the *In- situ* strain curvature of GaN grown on SiO_2 with the MLG layer, the feasibility of the curvature monitoring system in PSD was tested. To do so, the anisotropic two-dimensional curvatures of *a*-GaN grown on *r*-plane sapphire were measured using the curvature measurement system in PSD. The *a*-GaN has two different lattice parameters, which are perpendicular to each other as shown in Figure 3-5.

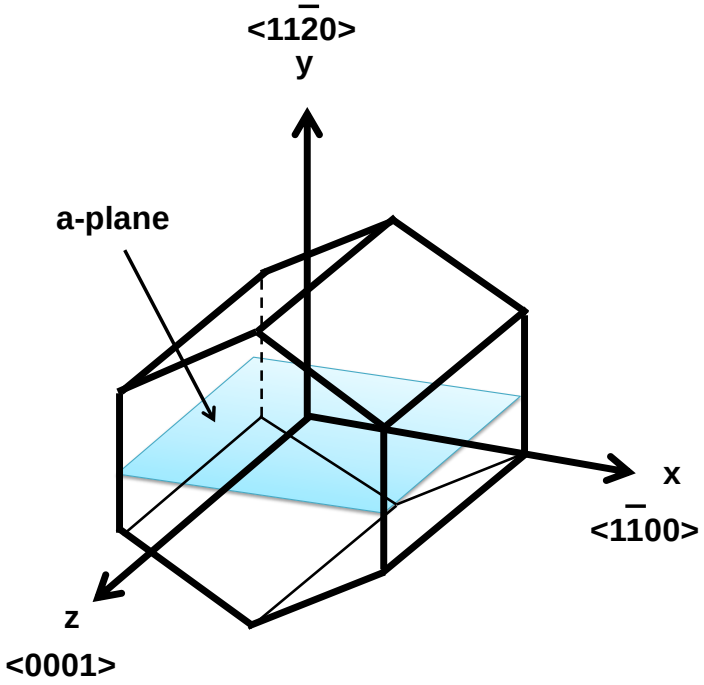

Figure 3-5 Spatial structure of a-GaN.

To measure the two-dimensional curvatures, two etalons between the sample and laser were installed. On the other hand, this set-up of etalons results in lower laser intensity because the laser signal, which has passed through the etalon, is a separated spot. These low intensity and separated spot laser signals generate additional errors in the measurements. The errors were reduced by adjusting the exposure time of the detector and optical power.

GaN films were grown under Ga-rich conditions on 2-in r-plane sapphire substrates by PSD. Before introducing the substrates to the PSD chamber, the sapphire substrates were annealed at 800 °C for 60 min to remove contaminants of the substrate in vacuum. The substrates were then introduced into the PSD chamber with a background pressure of 1.0×10^{-10} Torr. The growth temperature was set at 800 °C, which was calibrated using a pyrometer. Sputtering of the Ga target was performed in a N_2/Ar gaseous ambient. The ambient N_2

activated by the pulsed discharge was used as the nitrogen source. Pulsed dc power was applied at 20- 100W.

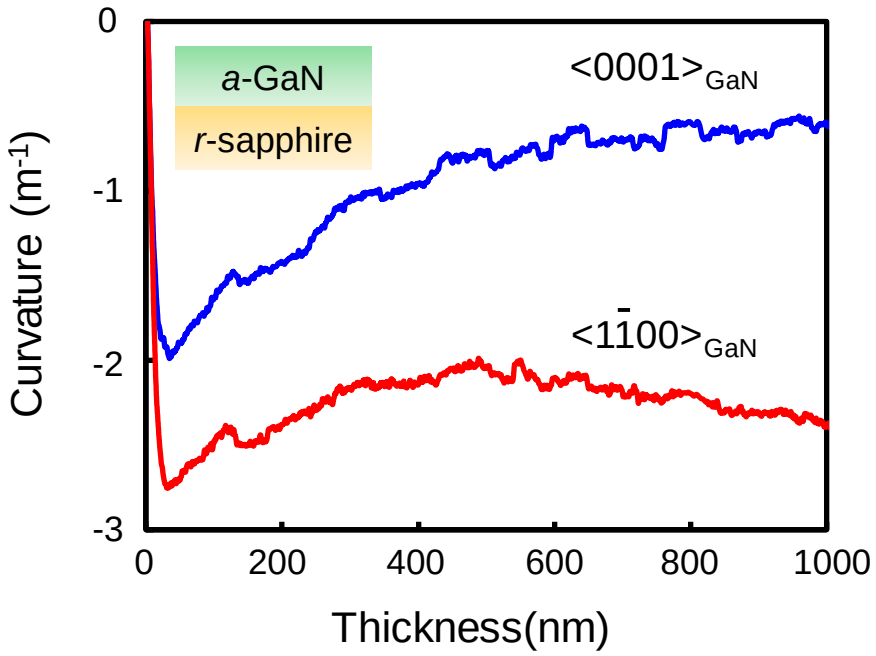

Figure 3-6 *In- situ* curvature measurements for *a*-GaN growth.

Figure 3-6 shows the change in curvature during GaN growth. The results clearly show different trends along the two perpendicular directions, $[0001]_{GaN}$ and $[1\bar{1}00]_{GaN}$, respectively. This anisotropic curvature change is mainly caused by the difference in the generation of misfit dislocations owing to the anisotropy in the lattice mismatch between GaN and sapphire (1.3 and 16.2% along $[0001]_{GaN}$ and $[1\bar{1}00]_{GaN}$, respectively).

3.4 Strain measurements of GaN grown on SiO_2 with MLG by PSD

3.4.1 *In- situ* curvature measurements of GaN grown on SiO_2 with MLG by PSD

The *In- situ* curvature measurements were performed during GaN growth on SiO_2 with MLG layers by PSD. The change of the wafer curvature was monitored for the GaN growth on SiO_2 with MLG layers and on conventional c-plane sapphire substrates. The slope of the curvature change as a function of growth time explains the generation of the stress between the film and substrate as the film thickness increases. Negative and positive slopes of the curvature in mean compressive stress and tensile stress, respectively. The curvature during the GaN growth on sapphire showed rapid changes toward negative values, which indicates the generation of compressive strain in the GaN films. The large compressive strain in the GaN films on sapphire is mainly caused by the lattice mismatch between GaN and the sapphire substrates. On the other hand, the change in the curvature during GaN growth on SiO_2 with the MLG buffer layers was quite small, indicating the small strain in the GaN films.

3.4.2 *Ex- situ* strain measurements of GaN grown on SiO_2 with MLG by PSD

The strain was also investigated by *ex- situ* XRD. The c-axis lattice constant of the GaN films was determined from the $2\theta/\omega$ XRD peaks, as shown in Figure 3-7. The c-axis lattice constant, c_h, is determined from the angular position of the 000h diffraction peak, and c_r was

determined from the plot $\{p_h, c_h\}$ according to the standard extrapolation using Equations 3-10, 3-11, and 3-12.

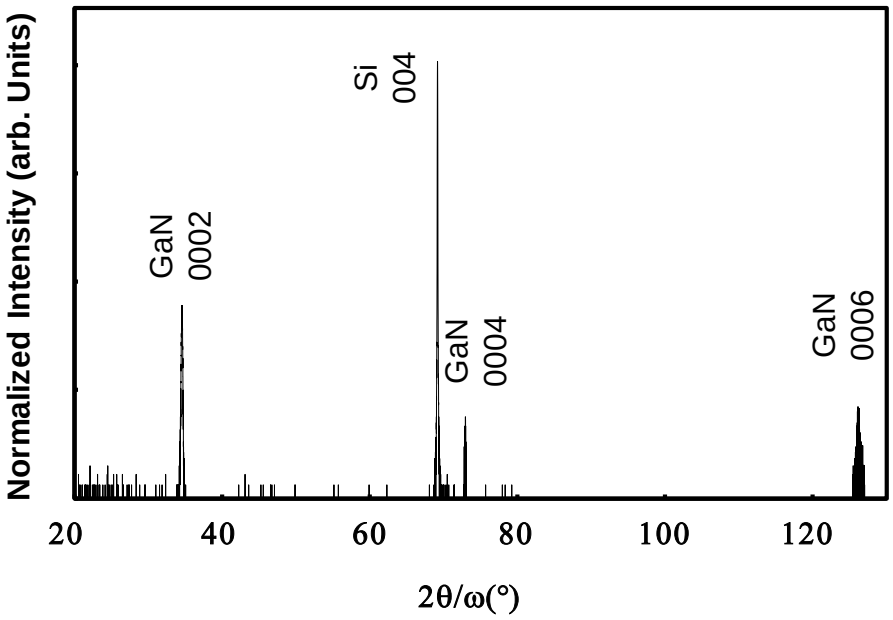

Figure 3-7 XRD curve of the GaN films grown on MLG/SiO_2 layers

Figure 3-8 shows *ex- situ* strain measurements GaN films grown on various substrates with a range of thicknesses. The *ex- situ* measurements also showed that GaN films on the MLG layers have less strain than GaN films on sapphire, which agrees with the results of the *In- situ* measurement. The strain in the GaN films grown on sapphire was as large as 1%, whereas that on SiO_2 with MLG buffer layers was < 0.4 %. GaN films grown on MLG/SiO_2 both with and without an AlN interlayer have a small amount of strain even when the thickness is increased.

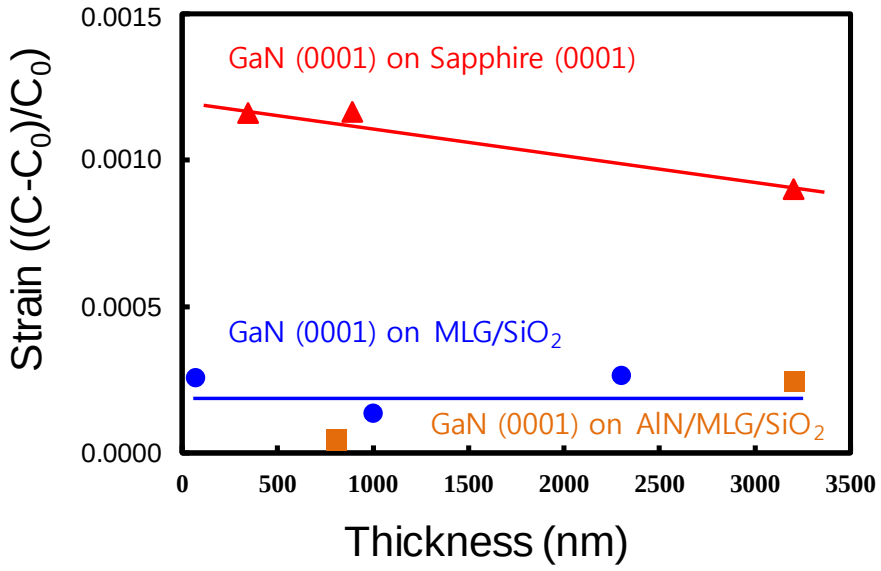

Figure 3-8 *Ex- situ* strain measurement of GaN.

The strain components in the GaN layer are the superposition of the biaxial and hydrostatic strain, which can be evaluated using symmetric and asymmetric XRD measurements. On the other hand, GaN films grown on SiO_2 substrate with MLG layers do not have sufficient crystal quality for asymmetric XRD measurement due to the coexistence of wurtzite and zincblende phase GaN. Therefore, asymmetric XRD measurements of the GaN films grown on MLG/SiO_2 substrate with AlN interlayer were performed because, as mentioned above, the insertion of AlN between GaN and the MLG buffer layer improves the phase purity and crystal quality. GaN films grown on sapphire substrate were chosen as reference.

As mentioned in section 3.3.1, the in-plane lattice constants were evaluated from the XRD peaks of the asymmetric reflections hkil = $10\bar{1}4$, $10\bar{1}5$ and $20\bar{2}4$. The real values of the a-lattice constant, a_r, and its experimental values, a_h, are connected through the angular parameter, p_{hkil},

by the relationship represented in Equations 3-13, 3-14, and 3-15. From those lattice constants, the combination of ε_c, ε_a leads to biaxial strain, ε^b_c, ε^b_a, and hydrostatic strain, ε_h.

	Measured		Hydrostatic	Biaxial	
	$e_c(10^{-3})$	$e_a(10^{-3})$	$e_h(10^{-3})$	$e_c^b(10^{-3})$	$e_a^b(10^{-3})$
Sample 1	0.06	-1.15	-0.36	0.42	-0.79
Sample 2	1.20	-7.75	-1.91	3.11	-5.84

Table 3-1 Strain in GaN films grown on AlN/MLG/SiO_2 and sapphire

Table 3-1 shows the strain component in GaN films grown on AlN/MLG/SiO_2 (Sample 1) and sapphire (Sample 2). The GaN films in both samples show that the measured and the biaxial out-of-plane strain are of the tensile type, whereas the in-plane strains are of the compressive type. As shown in Table 3-1, the deformation of Sample1 is approximately one order of magnitude lower than Sample 2 in both hydrostatic and biaxial strain.

Ishii's group recently reported the results of a theoretical investigation of GaN growth on graphene as shown Figure 3-9 [3.20].

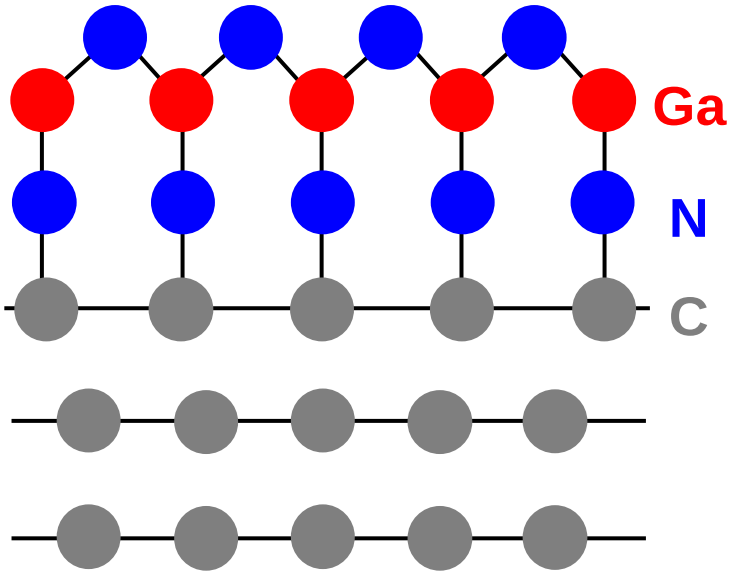

Figure 3-9 Schematic diagram of epitaxial growth of GaN on graphene [3.20].

The interaction between each graphene layer is relatively weak; thus. van der Waals forces dominate the interaction [3.20] and the change in the topmost layer does not propagate to the under layer. Only the topmost layer of the MLG is extended to have a longer lattice constant that is equal to the GaN, whereas the under layers are not extended because of the two-dimensionality of graphene. Most of the deformation is absorbed at the topmost layer of the MLG and only small amounts of strain are generated on the GaN films.

In the case of single graphene, the simulation indicated that the interface interactions of the graphene/a-SiO_2 (0001) were 77 meV/C atom, hence van der Waals forces dominate the interaction [3.21]. The two-dimensionality of graphene might explain the small amount of GaN strain during the *In- situ* measurement.

3.5 Summary

This chapter covers the development of the *In- situ* curvature measurement system for group III-nitride films grown by PSD. The reliability of the measurement system was confirmed by measuring the in-plane anisotropic strain of *a*-GaN films grown on *r*-sapphire substrates. The results clearly show different trends along the two perpendicular directions, $[0001]_{GaN}$ and $[1\bar{1}00]_{GaN}$, respectively

The *In- situ* curvature measurements of GaN films grown on MLG buffer layers indicated less strain than that on the sapphire substrates. The *ex- situ* XRD measurements also showed a small amount of in-plane and out-of-plane strain in the GaN films grown on the MLG layers.

Because of the two-dimensionality of graphene, most of the strain that is generated by the difference in lattice mismatch is absorbed on the topmost layer of the MLG and only a small amount of strain was generated on the GaN films.

[3.1] W. D. Nix, Metallurgical Transactions A **20A**, 2217 (1989).

[3.2] W. D. Nix, and B. M. Clemens, J. Mater. Res. **14**, 3467 (1999).

[3.3] R. W. Hoffman, Thin Solid Films **34**, 185 (1976).

[3.4] B. W. Sheldon, A. Rajamani, A. Bhandari, E. Chason, S. K. Hong, and R. Beresford, J. Appl. Phys. **98**, 043509 (2005).

[3.5] P. Chaudhari, J. Vac. Sci Techno. **9**, 520 (1971).

[3.6] M. F. Doerner, and W. D. Nix, Crit. Rev. Solid State Mater. Sci. **14**, 225 (1988).

[3.7] R. Koch, J. Phys.: Cond. Matt. **6**, 9519 (1994).

[3.8] S. Hearne, E. Chason, J. Han, J. A. Floro, J. Figiel, J. Hunter,H. Amano, and I. S. T. Tsong, Appl. Phys. Lett. **74**, 357 (1999).

[3.9] J. D. Acord, I. C. Manning, X. Weng, D. W. Snyder, and J. M. Redwing, Appl. Phys. Lett. **93**, 111910 (2008).

[3.10] C. Kisielowski, J. Kruger, S. Ruvimov, T. Suski, J. W. Ager III, E. Jones, Z. Liliental-Weber, M. Rubin, and E. R. Weber, Phys. Rev. B **54**, 17 745 (1996).

[3.11] V. S. Harutyunyan, A. P. Aivazyan, E. R. Weber, Y. Kim, Y. Park, and S. G. Subramanya, Weber, J. Phys. D: Appl. Phys. **34**, A35 (2001).

[3.12] A. Polian, M.Grimsditch, and J.Grzegory, J. Appl. Phys. **79**, 3343 (1996).

[3.13] G. G. Stoney, Proc. R. Soc. Lond. A. **82**, 172 (1909).

[3.14] S. Raghavan, J. Acord, and J. M. Redwing, Appl. Phys. Lett. **86**, 261907 (2005).

[3.15] S. Raghavan and J. M. Redwing, J. Appl. Phys. **96**, 2995 (2004).

[3.16] S. Raghavan and J. M. Redwing, J. Cryst. Growth, **261**, 294 (2004)

[3.17] A. Krost, A. Dadgar, F. Schulze, J. Blasing, G. Strassburger, R. Clos, A. Diez, P. Veit, T.

Hempel, and J. Christen, J. Cryst. Growth, **275**, 209 (2005)

[3.18] Y. Cordier, N. Barona, F. Semond, J. Massies, M. Binetti, B. Henninger,M. Besendahl, and T. Zettler, J. Cryst. Growth, **301**, 71 (2007)

[3.19] J.F. Geisz, A.X. Levander, A.G. Norman, K.M. Jones, and M.J. Romero, J. Cryst. Growth, **310**, 2339 (2008)

[3.20] A. Ishii, T. Tatani, H. Asano, and K. Nakada, Phys. Status Solidi C **7**, 347 (2010).

[3.21] Z. Ao, M. Jiang, Z. Wen, and S. Li, Nanoscale Res. Lett. **7**, 158 (2012).

Chapter 4

Fabrication of the GaN-based LEDs using MLG buffer layers on amorphous SiO_2

4.1 Introduction

As discussed in Chapter 1, several research groups have reported the growth of group III-nitride LED structures on amorphous substrate [4.1-4.3]. Recently J. H. Choi *et al.* reported the fabrication of the GaN LEDs on amorphous fused silica glass substrates with MOCVD [4.3, 4.4]. The group used a 'pre-orienting titanium layer' and SiO_2 mask layers to achieve nearly single-crystalline GaN pyramid arrays on the amorphous fused silica glass substrates. They are represented as blue and green LED s. The growth temperature of GaN (1040 °C) in this method, however, was too high for conventional glass substrates.

In chapter 2, I discuss the successful growth of group III-nitride films on amorphous SiO_2 substrate with MLG. A reduction in the GaN growth temperature was possible in the case of PSD. This chapter reports the results of tests examining the feasibility of group III-nitride LEDs on SiO_2 with MLG buffer layers by PSD.

4.2 Experimental procedure

The MLG layers were grown by CVD, followed by transfer onto 100-nm-thick SiO_2/Si (100). Before the growth of group III-nitride films, the MLG/ SiO_2/Si substrates were degassed at 600 °C for 30 min in a vacuum. The growth of InGaN, GaN and AlN films were performed using a PSD apparatus with a background pressure of 1.0×10^{-10} Torr. The GaN films were grown at 760 °C after the growth of 50-nm-thick AlN layers. The surface of the AlN inter interlayers were thermally oxidized at 200 °C in air to form AlOx layers, which leads to the formation of Ga-polar GaN films. The InGaN films were deposited at 500-650°C. The sputtering of metal targets such as In, Ga and Al was performed in a N_2/Ar gaseous ambient. The growth rate of GaN films was 1.0 um/hr. To fabricate the LED structures, five periods of InGaN/GaN multiple quantum wells (MQWs) and Mg-doped p-type GaN layers were grown on n-type GaN layers. The thickness of the MQWs and p-type GaN was 60 nm and 600 nm, respectively. The samples were characterized by X-ray diffraction (XRD), scanning electron microscopy (SEM), photoluminescence (PL), and electroluminescence (EL). Figure 4-1 shows a schematic diagram of these LED structure samples.

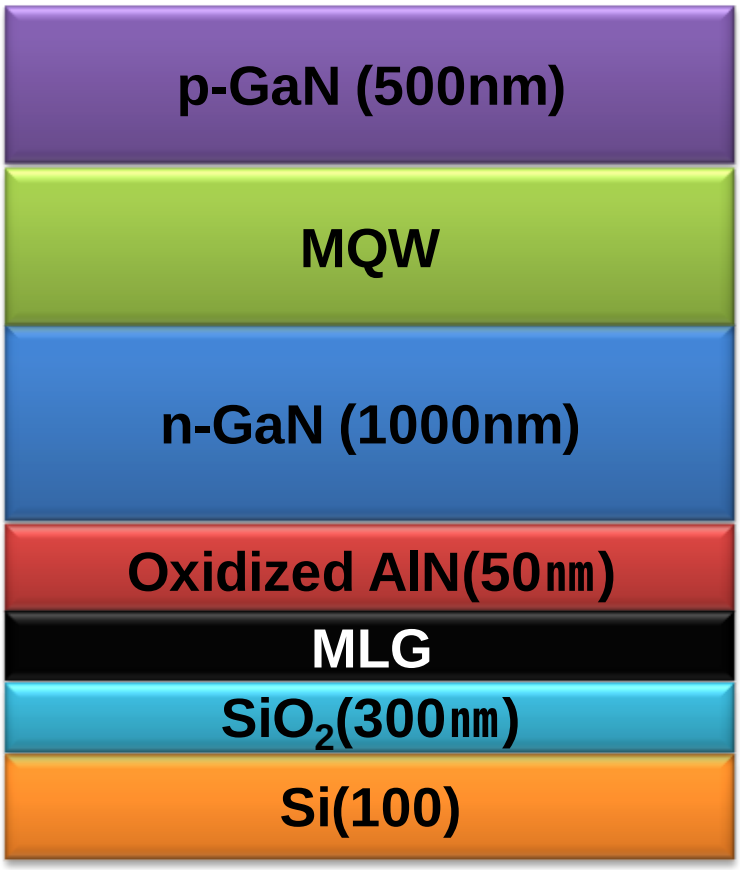

Figure 4-1 Schematic diagram of the LED structure.

4.3 Structural analysis of the LED structure

Figure 4-2 shows a 2θ/ω XRD scan of the LED structure. The XRD peaks were observed at approximately 26.5°, 34.5°, 36.0°, 69.1°, and 72.9°. These peaks correspond to the XRD peaks from MLG 0002, GaN 0002, AlN 0002, Si 400, and GaN 0004, respectively and suggest that the AlN and GaN films have highly *c*-axis oriented structures.

Figure 4-3 shows the experimental XRD 2θ/ω scan data (black line) and theoretical fitting (red line). The satellite peaks around the GaN 0002 diffraction peak in the XRD curves indicated the smooth and abrupt interfaces of the MQWs. The fitting to the experimental curves revealed that the MQWs structure consists of five layers of 3.1-nm-thick $In_{0.21}Ga_{0.79}N$ wells and five layers of 8.6-nm-thick GaN barriers. Figure 4-4 (a) shows the structure of these MQWs and Figure 4-4 (b) shows band structure of MQW.

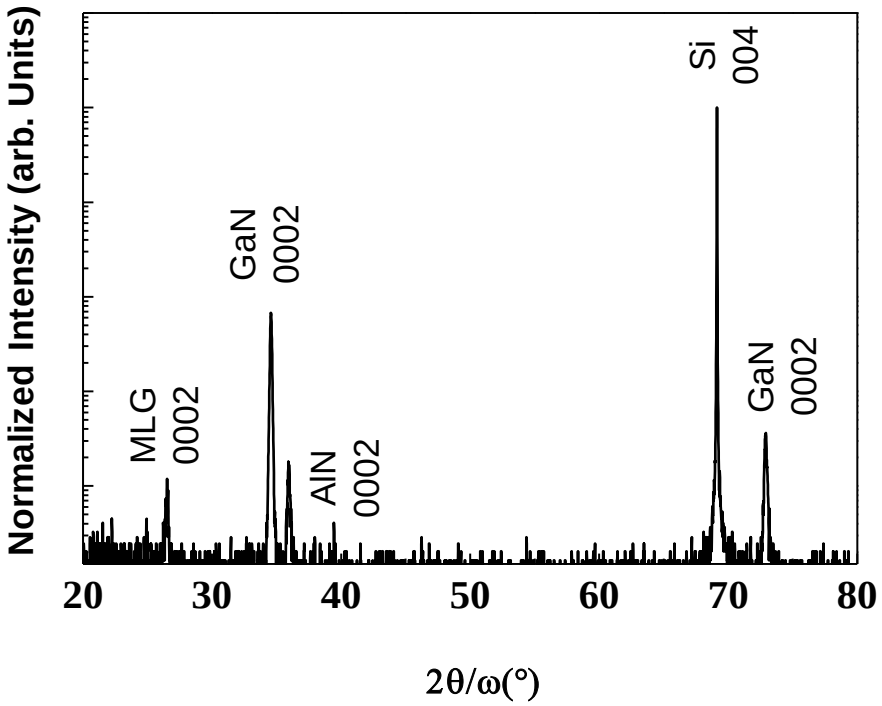

Figure 4-2 XRD curve of the LED structure.

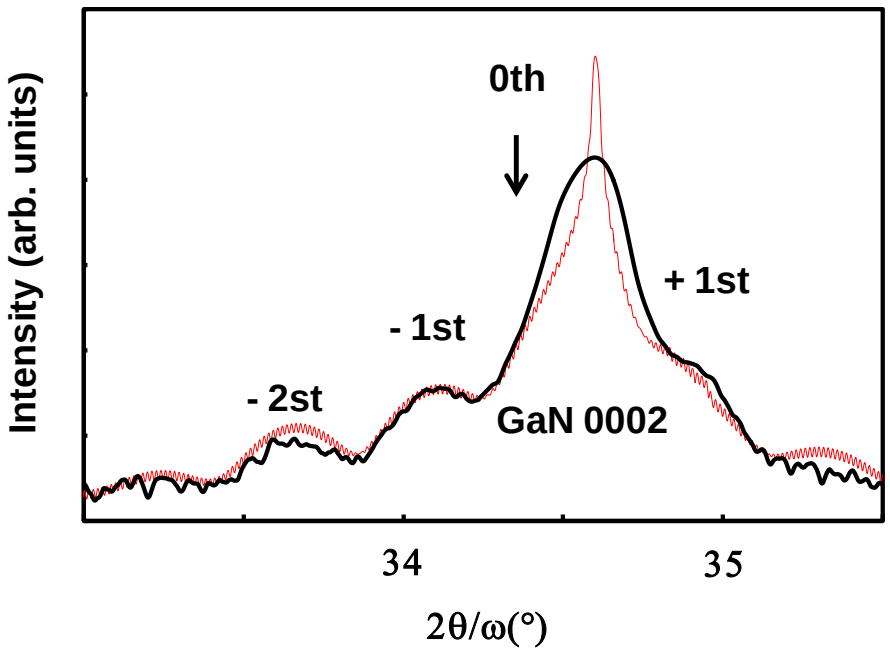

Figure 4-3 XRD curve of LED structure around GaN 0002.

(a) (b)

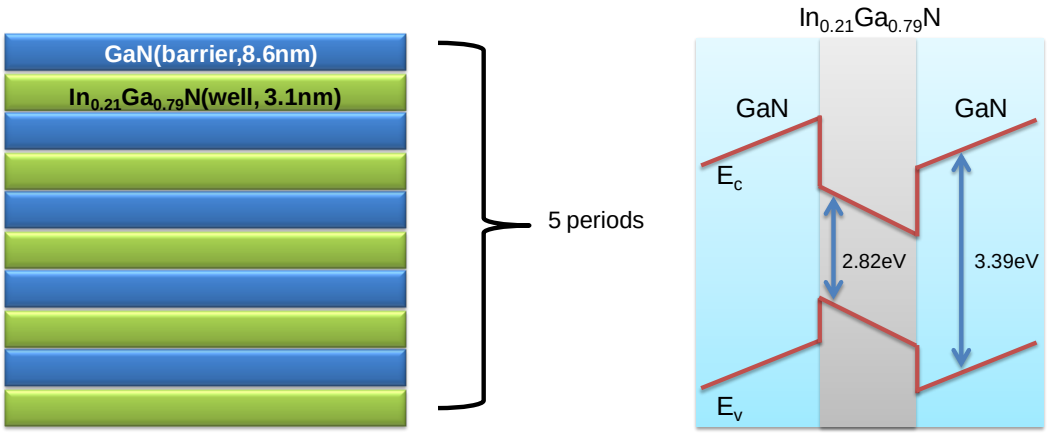

Figure 4-4 (a) Schematic diagram of the MQWs structure,

(b) Band structure of MQW.

Figure 4-5 shows the EBSD phase mapping for the LED structure. The EBSD phase mapping shows only a wurtzite phase GaN signal and that the insertion of AlN inter layer effectively suppresses the growth of zincblende phase GaN.

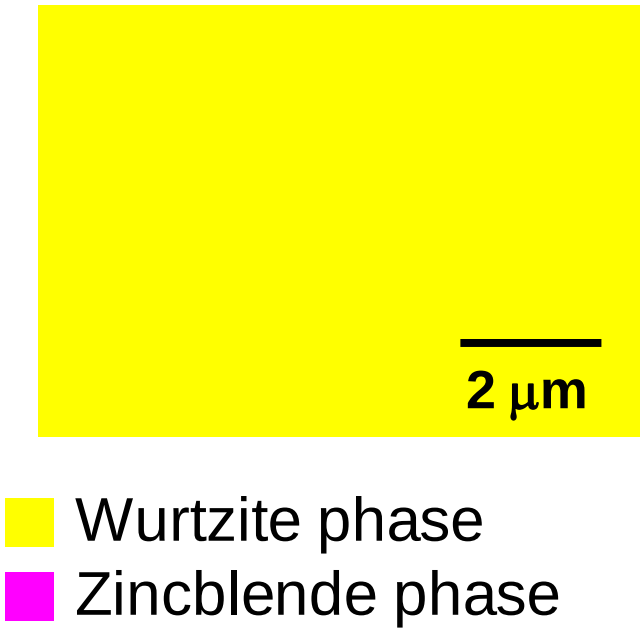

Figure 4-5 EBSD phase map of the GaN film grown on MLG/SiO_2 layers.

The previous chapter reported that the use of a thermally oxidized AlN interlayer produces Ga-polar GaN films with flat surface. The image of the LED structure (Figure 4-6 (a)) generally resembles the Ga-polar GaN images. Furthermore, the surface morphology of the LED structure remained unchanged after KOH etching as shown in Figure 4-6(b). This unchanged surface morphology indicates the formation of Ga-polar GaN films [4.5]. The results showed that Ga- polar and flat surface LED structures could be grown on amorphous substrates with MLG buffer layers.

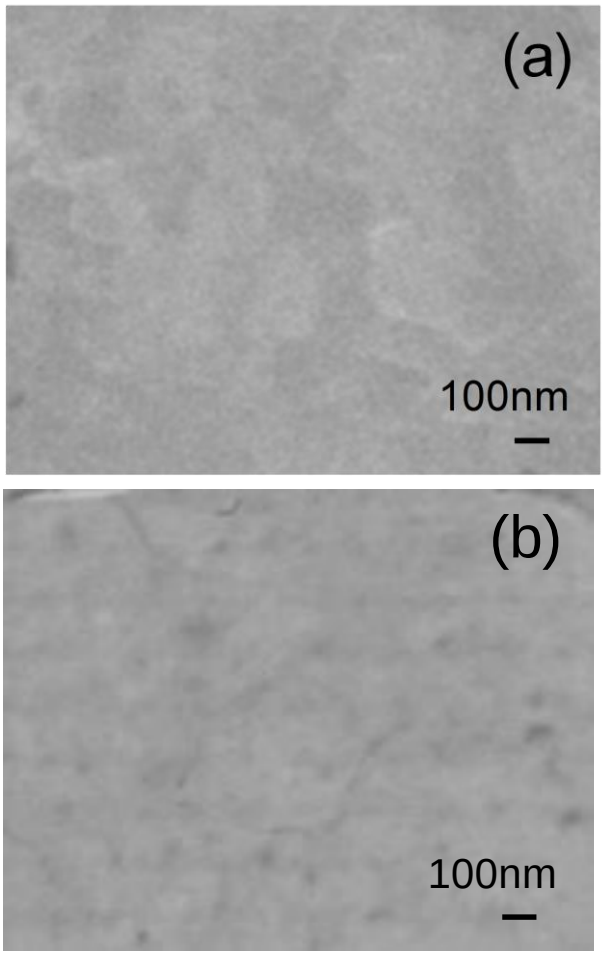

Figure 4-6 SEM images of the LED structure, (a) before and (b) after KOH etching.

4.4 Optical properties of the LED structure

4.4.1 PL measurements of the LED structure

Before fabricating LEDs on the amorphous substrates, a feasibility study of the growth of InGaN/GaN MQWs on amorphous substrates must be conducted. Therefore, MQWs were

grown on GaN/AlO_x/AlN/MLG/amorphous SiO_2 at different growth temperatures by PSD. The optical properties of the MQWs were investigated by measuring the PL spectra using a He-Cd laser (λ = 325 nm) and violet semiconductor laser (λ = 405 nm) as the excitation sources. Three samples were grown at different MQW growth temperatures: sample A (setting temperature 660°C: blue), sample B (setting temperature 630°C: green) and sample C (setting temperature 610°C: red). With decreasing growth temperature, the peak wavelengths of the PL emission of group III-nitride MQWs varied from blue to red. Figure 4-7 shows the RT-PL spectra of three different InGaN/GaN MQWs. The PL spectra of the InGaN/GaN MQW structures strongly depend on the growth temperature [4.6–4.8]. The increase in the growth temperature of MQWs increases the desorption of indium because the bonding energy of InN is lower than that of GaN [4-9–4.11]. Therefore, the indium content in InGaN films increases with decreasing growth temperature and a red shift in the PL peak is observed with decreasing growth temperature.

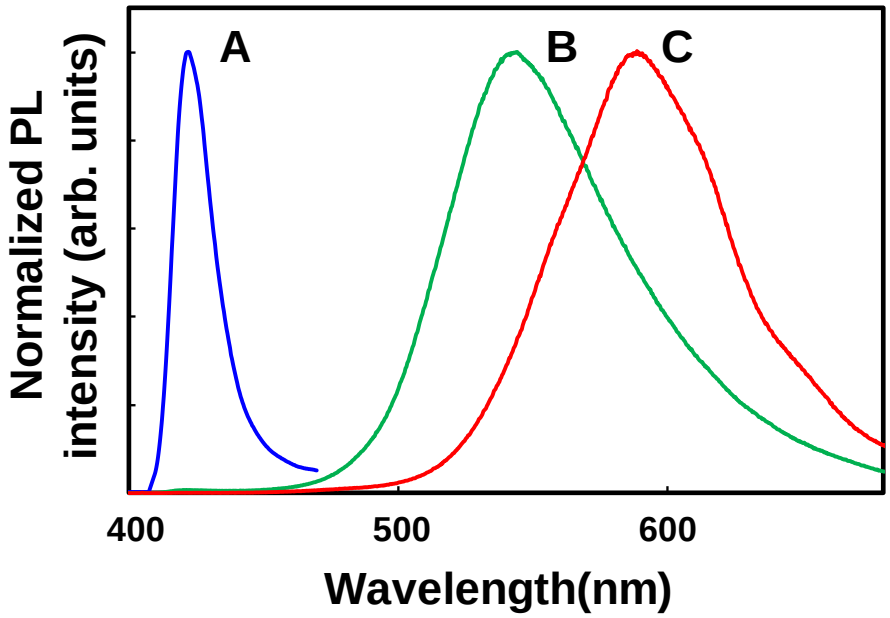

Figure 4-7 RT PL spectra for MQW samples, A, B and C.

The green luminescence of sample B was clearly observed at the peak wavelength of 520 nm. Figure 4-8 shows the PL spectra of blue commercial LED and green MQW structure sample B. The integrated intensity of luminescence from the MQW structure sample B was approximately 14 % compared with the blue luminescence from a commercially available blue LED whose internal quantum efficiency (IQE) was approximately 50 %.

With sample B, the IQE of the MQW structure grown on GaN/AlO_x/AlN/MLG/amorphous SiO_2 was identified. Figure 4-9 shows the temperature dependence of the integrated PL intensity. The IQE in the MQW active layers was calculated by dividing the integrated PL intensity measured at 300 K by the integrated PL intensity measured at 13 K. Because the PL intensities of both MQW structures were almost saturated at the measured temperatures below 50K, it was assumed that the recombination efficiency of the photo-excited electrons and holes was almost 100% at 10 K [4.12, 4.13]. The integrated PL intensity ratio (I_{300K}/I_{13K}) is defined as the IQE in the MQW. This shows that the ratio of the integrated PL intensity at 13 K to that at 300 K is 7.4 %, which is comparable to the values, conventional InGaN QW is 17.3%, on the green LEDs on conventional sapphire substrates [4.14, 4.15, and 4.16]. We have not yet measured the luminous efficiency of white-light emission or the external quantum efficiency of a single color.

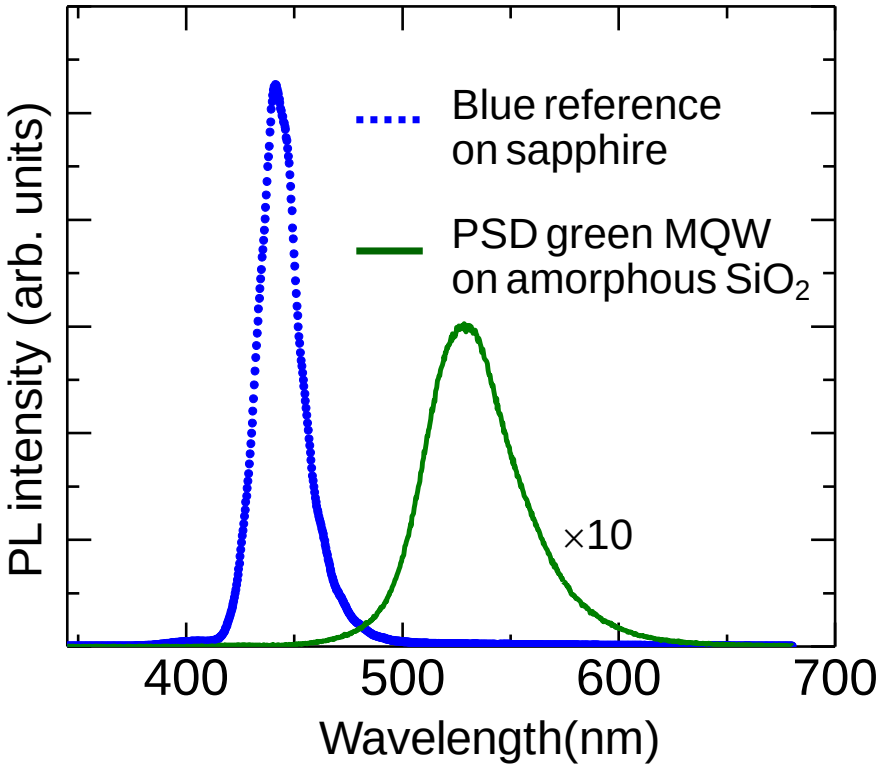

Figure 4-8 PL spectra of commercial blue reference LED and MQW structure sample B.

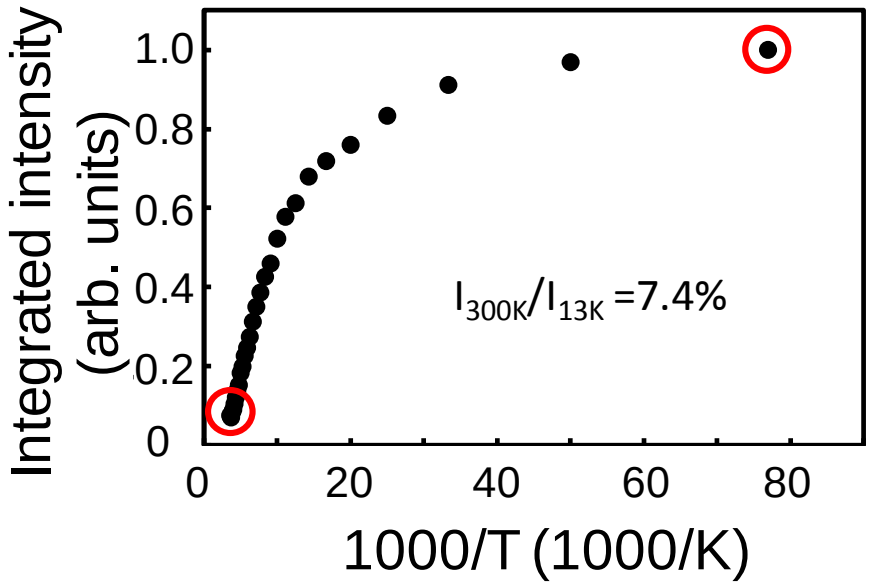

Figure 4-9 Temperature dependence of the integral PL intensities of the MQW structure (Sample B).

4.4.2 EL measurements of the LED structure

After the deposition of Pd/Au and In electrodes on p- and n-type GaN surfaces, the electroluminescence (EL) spectra of the LED sample were measured. Figure 4-10 shows the structures of the LED grown on amorphous SiO_2 substrates with the MLG buffer layers. This sample clearly demonstrated strong green light as the green light could be recognized by the naked eye under normal illumination conditions. Figure 4-11 shows the EL spectra of the LEDs grown on SiO_2 with the MLG buffer layers. The EL intensity increased gradually with increasing injection current from 2.1 to 10.8 mA. The successful LED operation suggests that group III-nitride LEDs can be grown directly on large size and flexible amorphous substrates.

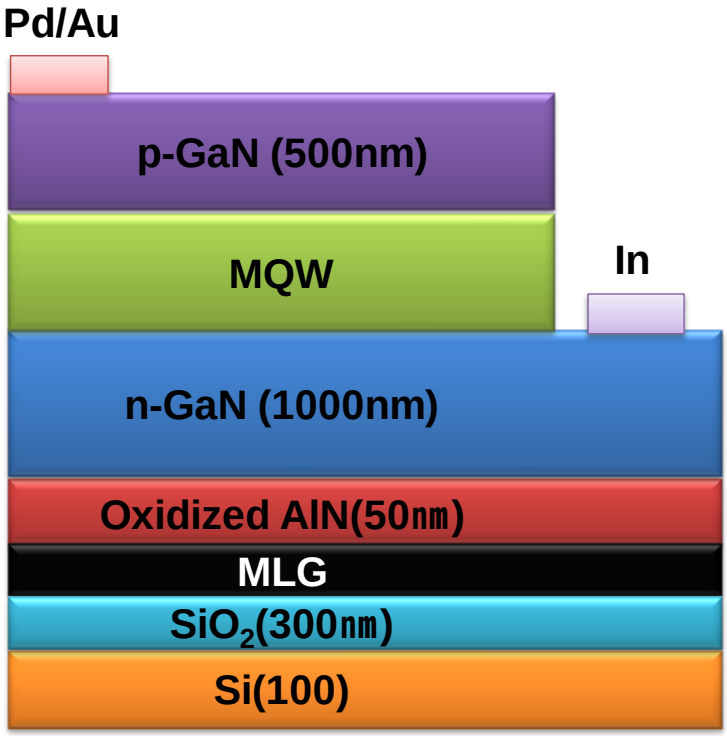

Figure 4-10 Schematic diagram of the LED fabricated on amorphous SiO_2 substrate with MLG buffer layers.

As mentioned above, the peak wavelength of MQW can be controlled by adjusting the MQW growth temperature. Blue and red LEDs were successfully produced by changing the MQW growth temperature in the MQWs as shown in Figure 4-12. These colour variation of the LED samples suggest that group III-nitride LED grown on amorphous substrate can cover the entire visible light range.

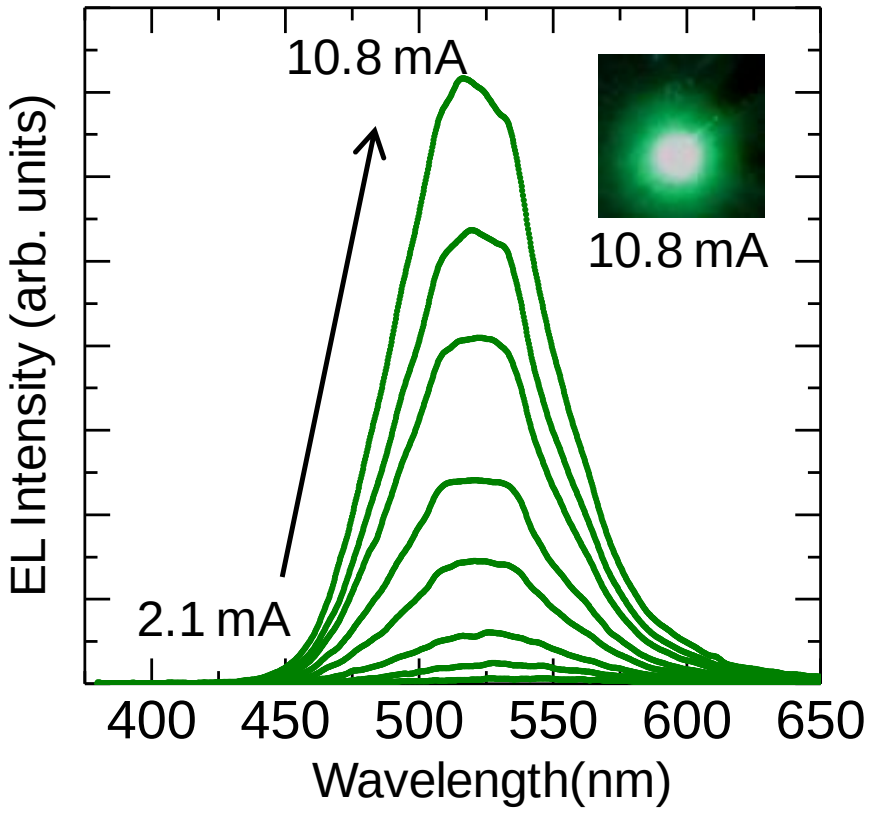

Figure 4-11 Green EL spectra of the LED grown on SiO_2 with MLG buffer layers.

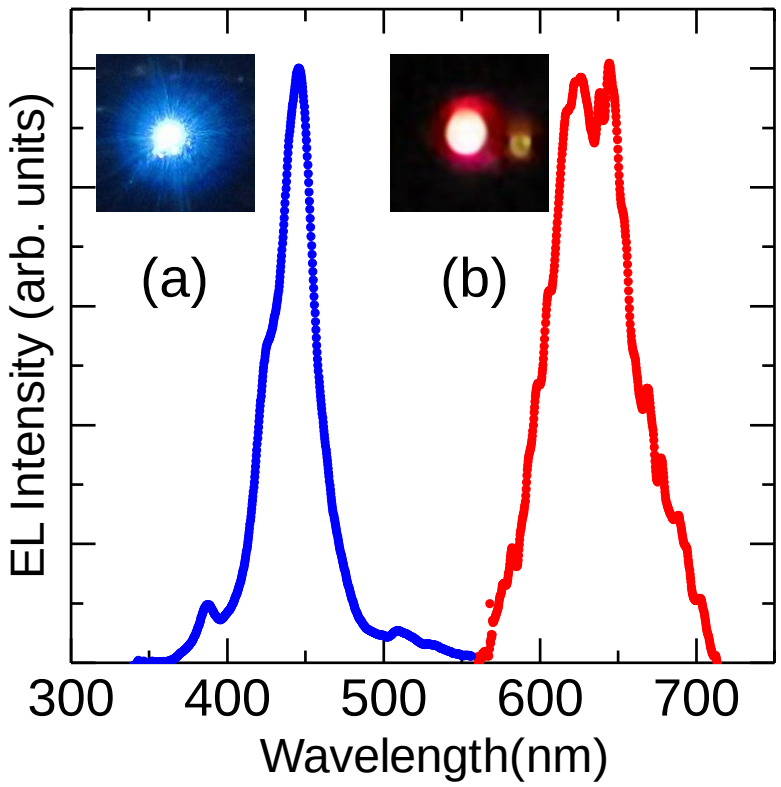

Figure 4-12 EL images of the LEDs with different growth temperature (a) blue (b) red.

4.5 Summary

Based on the knowledge described in Chapter 2, GaN-based LEDs were fabricated on amorphous SiO_2 substrates with MLG buffer layers. The use of MLG buffer layers improves the crystalline quality of the LED structure dramatically. The insertion of oxidized AlN interlayers between the GaN and MLG layer led to the formation of Ga-polar GaN. The LEDs exhibited clear EL emissions. The colour of LED could be changed from blue to red by adjusting the growth temperature of MQWs. The results suggest that the present technique is a promising method for fabricating large-area and flexible devices based on group III-nitrides.

[4.1] D. P. Bour, N. M. Nickel, C. G. Van de Walle, M. S. Kneissl, B. S. Krusor, P. Mei,and N. M. Johnson, Appl. Phys. Lett. **76**, 2182 (2000)

[4.2] K. Chung, S. I. Park, H. Baek, J. Chung, and G. Yi, NPG Asia Mater. **4**, e24 (2012)

[4.3] J. H. Choi, A. Zoulkarneev, S. I. Kim, C. W. Baik, M. H. Yang, S. S. Park, H. Suh, U. J. Kim, H. B. Son, J. S. Lee, M. Kim, J. M. Kim. and K. Kim, Nat. Photonics **5**, 763 (2011).

[4.4] J. H. Choi, H. Y. Ahn, Y. S. Lee, K. Park, T. Kim, K. S. Cho, C. W. Baik, S. I. Kim, H. Yoo, E. H. Lee, B. L. Choi, S. Kim, Y. Kim, M. Kim, and S. Hwang, J. Mater. Chem. **22**, 22942 (2012).

[4.5] J.L. Weyher, S. Miiller, I. Grzegory, and S. Porowski, J. Cryst. Growth **182**, 17 (1997).

[4.6] S. Nakamura, Solid State Commun. **102**, 237 (1997).

[4.7] F. Chen, A. N. Cartwright, P. M. Sweeney,M. C. Cheung,J. S. Flynn, and D. Keogh, MRS Proceedings **693**, I6.27. (2002).

[4.8] K. Shen, T. Wang, D. Wuu, and R. Horng, Opt. Express **20**, 15149. (2012).

[4.9] C. S. Gallinat, G. Koblmüller, J. S. Brown, and J. S. Speck, J. Appl. Phys. **102**, 064907, (2007)

[4.10] S. Keller, B. P. Keller, D. Kapolnek, U. K. Mishra, S. P. Denbaars, I. K. Shmagin, R. M. Kolbas, and S. Krishnankuty, J. Cryst. Growth **170**, 349 (1997).

[4.11] W. Van Der Stricht, I. Moerman, P. Demeester, L. Considine, E. J. Thrush, and J. A. Crawley, MRS Internet J. Nitride Semicond. Res. **2**, 16 (1997).

[4.12] W. Huang, C. Lin, T. Hsieh, S. Chen, M. Lin, K. Chen, C. Lin, S. Chen, and P. Han, Opt. Express **19**, A1126 (2011).

[4.13] K. Okamoto and Y. Kawakami, IEEE J. Sel. Top. Quantum Electron. **15**, 1199 (2009).

[4.14] M. Kumar, J. Park, Y. Lee, S. Chung, C. Hong and E. Suh, Jpn. J. Appl. Phys. **47**, 839, (2008)

[4.15] M. Liu, Optical Engineering **46**, 074002 (2007).

[4.16] H. Zhao, G. Y. Liu, J. Zhang, J. D. Poplawsky, V. Dierolf, and N. Tansu, Opt. Express 19, A991–A1007 (2011).

Chapter 5

Summary

This study examined the followings:

- Growth of group III nitride films on amorphous SiO_2 substrates with the MLG buffer layer by PSD
- The structural properties of group III nitrides on an amorphous SiO_2 substrate with the MLG buffer
- The strain state of GaN and AlN films on amorphous SiO_2 substrates with the MLG buffer
- Fabrication of GaN-based LEDs on amorphous SiO_2 substrate with MLG buffer layers.

Chapter 2 showed that group III-nitride films could be grown successfully on amorphous SiO_2 with MLG buffer layers by PSD due to the 2 dimentional crystal structure of graphene and the supply of high-energy film precursors in PSD. In addition, the structural properties of the GaN films on these substrates were examined. The *c*-axis oriented group III-nitride films could be grown on MLG buffer layers. On the other hand, the direct growth of GaN films on the MLG buffer layers result in low phase purity GaN because of the coexistence of zincblende and wurtzite phases in the GaN films. The interaction between GaN and carbon in graphene could explain this low phase purity. Therefore, an AlN interlayer was inserted between the GaN films

and MLG buffer layers to remove the direct contact. As expected, the insertion of AlN interlayers improves dramatically the phase purity, resulting in wurtzite GaN only. Growth of N-polar GaN films on AlN/MLG/SiO_2 was identified by KOH wet etching. An AlO_x layer on AlN was generated by thermal oxidation of the AlN layer, and acts as an 'inversion layer'. Using this thermally oxidized AlN layer, the GaN films grown on AlO_x/AlN/MLG/SiO_2 were Ga-polar.

Chapter 3 discussed the *in-situ* curvature measurement system of group III nitride films grown by PSD. The reliability of the measurement was also checked. The anisotropic strains of *a*-GaN grown on *r*-sapphire, which were generated at the initial stages of growth due to the anisotropy in the lattice mismatch between *a*-plane GaN and *r*-plane sapphire, was measured to check the measurement system. The *in-situ* curvature measurements, the GaN films grown on MLG buffer layers indicate a small amount of strain at the initial stages of growth. *Ex-situ* XRD measurements also reveal that a small amount of hydrostatic and biaxial strain accumulated in GaN films grown on the MLG layers. The theoretical investigation proposed the epitaxial growth of GaN on graphene with small strain. Because of the two-dimensionality of graphene, most of the strain generated by lattice mismatch was absorbed on the topmost layer of the MLG and a small amount of strain remains in the GaN films

Chapter 4 described fabrication of group III-nitride LEDs on an amorphous SiO_2 substrate with a MLG buffer layer. In the sample, strong light emission was observed, even by the naked eye, under normal illumination condition. The use of MLG buffer layers improves dramatically the crystalline quality of the LED structure. The insertion of oxidized AlN interlayers between the GaN and MLG layers confirmed the Ga-polar group III-nitride LEDs. The IQE of the

MQWs grown on an amorphous SiO_2 substrate with MLG buffer layers was 7.4 %, which is comparable with the value for conventionally fabricated green MQWs on sapphire substrates. The LEDs exhibited clear EL emissions and the color of the LEDs was changed from blue to red by adjusting the growth temperature of MQWs.

The author extracts the following essentials for obtaining high-quality group III nitride films on amorphous substrates from these results.

- Use of two dimensional crystalline buffer layers is essential to grow high crystalline quality nitride films. Graphene is a promising candidate as the crystalline buffer layers, since large-area graphene films with highly c-axis oriented structures are available and can be easily transferred onto foreign substrates.
- Formation of abrupt interfaces between group III nitrides and graphene leads to the improvement in the phase purity, the crystalline quality, and the surface morphology of the group III nitride films. Insertion of the AlN interlayers between GaN and graphene meets the requirement mentioned above.
- Polarity control of the GaN films should be achieved for the fabrication of device structures. It was found that the surface oxidization of AlN interlayers leads to formation of Ga-polar GaN film on graphene, which is preferable to LED fabrication.

Based on these findings, we have succeeded in the growth of high quality group III nitride films on amorphous SiO_2, and demonstrated the operation of full colar LEDs. We suggest that since sputtering is very frequently used in the liquid crystal display industry, it is an established process that could be adapted to fabricate large-area inorganic LED displays on glass substrates.

It should also be noted that state-of-the-art technology in the glass industry can offer roll-to-roll processing of flexible glass foils. The combination of these techniques can lead to the development of large-area flexible inorganic devices in the future.

Publication list

1. J. W. Shon, J. Ohta, K. Ueno, A. Kobayashi, and H. Fujioka, *Fabrication of full-color InGaN-based light-emitting diodes on amorphous substrates by pulsed sputtering*, Sci. Rep. **4**, 5325 (2014).

2. J.W. Shon, J. Ohta, K. Ueno, A. Kobayashi, and H. Fujioka, *Structural properties of GaN films grown on multilayer graphene films by pulsed sputtering*, Appl. Phys. Express. 7, 085502 (2014).

3. J.W. Shon, J. Ohta , K. Ueno, A. Kobayashi, and H. Fujioka, *Investigation of anisotropic wafer bending curvature in a-plane GaN films grown on r-plane sapphire substrates*, J. Cryst. Growth 424, 11 (2015).

Acknowledgment

I would like to thank my research advisor, Professor Hiroshi Fujioka, for giving me the opportunity to join his research group and for teaching me how to be a researcher. He has provided the support and resources for my research, as well as an enjoyable environment in which to work. With his support, I can continue pursuing interesting research topics such as material growth, device fabrication, and characterization, especially in group III-nitride materials.

I had the opportunity to work and learn from good research associate, Dr. Ohta. I am particularly appreciative of the time when he spent teaching me the technique as well as having insightful discussions about my work.

Dr. Kobayashi and Dr. Ueno taught me how to use instruments and gave me good advice. I would like to thank Ms. Takano for helping me with lithography and the warm ambience in the office. Ms. Oyamada was extremely helpful with nearly all office works. I would also like to thank all the student of the group of Prof. Hiroshi Fujioka who gave me only good memories. I appreciate Ms. Kim Hye-Ryun for her help and sharing her time in the laboratory.

I want to thank all my family members including my mother and my sister. Without their unconditional love and support I could never have achieved this goal. I especially thank my wife, Eun Ok. She is a great source of inspiration to me, and I love her deeply.

When I first arrived in Japan and joined the group of Prof. Hiroshi Fujioka, I was worried about everything. Now I have only memories of good people and happy impressions. Thank you all for the great opportunity at the University of Tokyo and Japan.